Yarmouk University

Hijjawi Faculty for Engineering Technology

Computer Engineering Department

Intensity Based Triangular Fringe Projection Technique for Surface Profilometry Measurements

This Thesis was Submitted to the Department of Computer Engineering in Partial Fulfillment of the Requirements for the Master's Degree of Science of computer engineering/Industrial automation at Yarmouk University

By

Mohammad Abdullah Mohammad Bawaneh

Supervisor

Dr. Sami Al-Hamdan

July, 2017

المنارة للاستشارات

www.manaraa.com

Intensity Based Triangular Fringe Projection Technique for Surface Profilometry Measurements

By

Mohammad Abdullah Mohammad Bawaneh

This Thesis was submitted to the department of Computer Engineering in Partial Fulfillment of the Requirements for the Master's Degree of Science in Computer Engineering/Industrial Automation.

Signature of Author: _____

Committee Member	**Signature and Date**
Dr. Sami F. Al-Hamdan (Chairman) Associate Professor, Computer Engineering, Yarmouk University	٢٠١٧/٧/١٨
Dr. Mohammad A. Al-Jarrah (Member) Associate Professor, Computer Engineering, Yarmouk University	
Dr. Ahmed Musa (External Examiner) Associate Professor, Communications Engineering, Yarmouk University	

المنارة للاستشارات
www.manaraa.com

Dedication

This thesis is dedicated to:

My beloved Parents, Abdullah Bawaneh and Amal Jaradat. This could never be done without your support. Thank you for everything, no words can describe you. I wish that this will make you happy and proud of me. I will never forget your constant encouragement from I was a child until now.

My brothers, friends and all of people who cared about me and who always support me in my life.

www.manaraa.com

Acknowledgment

I would like to express my sincere gratitude to my advisor Dr. Sami Al-Hamdan for the support of my master research, for his patience, and for every thing I learned from him. His guidance has helped and taught me how to do research and how to write in a scientific manner. This could not have been done without his constant support and instructions.

Special thanks to everyone helped me in the equipment and the preparation of the setup of the practical part in this research: Abdullah Obeidat, Mohammad Saleem, Doaa Al-Sha'bi, Emran Abu-Jaleel, Yousef Khamaiseh, and Laith Ballout

Finally, I must express my gratitude to all my family members and to all my friends for providing me with support and continuous encouragement throughout these years of study. Thank you.

www.manaraa.com

Table of Contents

Title	Page
Committee Decision	I
Dedication	II
Acknowledgment	III
Table of Contents	IV
List of Figures	VIII
List of Tables	XIII
List of Abbreviations	XIV
Abstract	XV

Chapter 1: Introduction 1

1.1 What is 3D shape measurement 1

1.2 Fringe Patterns 4

1.2.1 Sinusoidal Fringe Patterns 4

1.2.2 Binary Patterns 5

1.2.3 Saw Tooth Fringe Patterns 6

1.2.4 Triangular Fringe Patterns 6

1.3 Motivation and Problem Statement 7

1.4 Contribution 9

1.5 Thesis Organization 9

Chapter 2: Literature Review 10

www.manaraa.com

Chapter 3: Methodology and Approach 18

3.1 Triangular Fringe Generation and Projection 18

3.2 The Selection of Triangular Fringe Patterns 19

3.3 Mathematical Derivation of Heights 22

Chapter 4: Simulation 28

4.1 Simulation with Ideal Conditions 28

4.1.1 Simulation of Semi-Sphere Object 28

4.1.2 Simulation of Car Roof Object 31

4.1.3 Simulation of Pyramid object 32

4.2 Simulation with an Added Random Noise 34

4.2.1 Simulation of Semi-Sphere with an Added Noise 35

4.2.2 Simulation of Car Roof with an Added Noise 41

4.2.3 Simulation of Pyramid with an Added Noise 46

4.3 Error Analysis 51

4.3.1 Error Analysis for Semi-Sphere Simulation 51

4.3.2 Error Analysis for Car Roof Simulation 52

4.3.3 Error Analysis for Pyramid Simulation 52

Chapter 5: Practical Experiment of Triangular Fringe Projection Technique 54

5.1 System Analysis and Experiment Procedure 54

5.1.1 Triangular Fringe Generation and Projection, and Image Acquisition 56

5.1.2 Image Pre-processing 57

www.manaraa.com

5.1.3 Height Calculations 59

5.1.4 Depth Calculation 60

5.1.5 Calibration Process 60

5.1.6 Algorithm steps 62

5.2 System Setup 62

5.3 Equipment specifications 64

5.4 Example of 3D Profilometry – Triangular shaped object 66

5.4.1 Image Reading and Cropping 68

5.4.2 Convert Image to Gray Level 69

5.4.3 Binarize Edges Images by Thresholding 70

5.4.4 Image Enhancement and Noise Removal 70

5.4.5 Load One Line 70

5.4.6 Height Calculations 71

5.4.7 Height Distribution 72

5.4.8 Height Calculations for the Whole Object 73

5.4.9 Calibration process 73

5.5 Practical Experiment result for curved paper object 74

Chapter 6: Discussion 76

6.1 Comparing between Triangular and Saw-tooth Techniques in the Simulation Experiment 77

6.2 Comparing between Triangular and Saw-tooth Techniques in the Practical Experiment 78

www.manaraa.com

6.3 Comparing the Used Computer with Several Computers in terms of Speed ... 81

Chapter 7: Conclusion, and Future Works 83

7.1 Conclusion 83

7.2 Future Works 84

References 85

Abstract (Arabic) 88

www.manaraa.com

List of Figures

Figure **Description** **Page**

Figure 1.1: 3D image for foot scanning. 1

Figure 1.2: Example of multi-camera passive 3D shape measurement system. 2

Figure 1.3: Example of an active 3D shape measurement system 3

Figure 1.4: Fringe projection profilometry system 4

Figure 1.5: One dimensional sinusoidal fringe patterns 5

Figure 1.6: Two dimensional Sinusoidal fringe patterns 5

Figure 1.7: One dimensional binary fringe patterns 5

Figure 1.8: One dimensional of saw tooth fringe pattern 6

Figure 1.9: Two dimensional of saw tooth fringe pattern 6

Figure 1.10: One dimensional triangular fringe patterns 7

Figure 1.11: Two dimensional triangular fringe patterns. 7

Figure 1.12: Cross sectional line intensity of an object 8

Figure 2.1: Marker attached laser projector-system configuration. 10

Figure 2.2: A scan from all viewpoints by moving the camera around the object. 11

Figure 2.3: The proposed system using four cameras. 12

Figure 2.4: The setup for the hybrid system proposed 13

Figure 2.5: Photograph of the test system. 14

Figure 2.6: Schematic diagram of 3D shape measurement system. 15

Figure 2.7: Triangular patterns projection experiments with two selected wavelength. 16

www.manaraa.com

Figure 2.8: Experiment setup of saw tooth projection 17

Figure 2.9: Saw tooth fringe patterns 17

Figure 3.1: Triangular wave form, amplitude = 250, period =64. 18

Figure 3.2: Triangular fringe patterns, amplitude = 250, period =128. 19

Figure 3.3: One line selection for saw-tooth fringe patterns. 20

Figure 3.4: One line selection for triangular fringe patterns..... 20

Figure 3.5: Tested image with two intensity levels 21

Figure 3.6: Intensity data of white and black image in theory 21

Figure 3.7: One line cross sectional of the captured image. 22

Figure 3.8: Schematic diagram for representation of ΔH (first half of the period). 22

Figure 3.9: Schematic diagram for representation of ΔH (second half of the period).... 25

Figure 4.1: The simulated semi sphere object. 29

Figure 4.2: The corresponding triangular fringe patterns. 29

Figure 4.3: The reconstructed object. 29

Figure 4.4: The absolute error of the simulation in the mid line of the object. 30

Figure 4.5: The simulated car roof object. 31

Figure 4.6: The corresponding triangular fringe patterns. 32

Figure 4.7: The reconstructed object. 32

Figure 4.8: The original pyramid object. 33

Figure 4.9: The corresponding fringe patterns..... 33

Figure 4.10: The reconstructed object. 33

www.manaraa.com

Figure 4.11: A 5 X 5 window of the special filter and the weights for every pixel 34

Figure 4.12: The original object. 36

Figure 4.13: Noisy fringe patterns with different standard deviations of noise. 37

Figure 4.14: Filtered fringe patterns by weighted mean filter. 38

Figure 4.15: Reconstructed objects with the different standard deviations of noise. 39

Figure 4.16: Applying mean filter on the reconstructed objects..... 40

Figure 4.17: The original car roof object. 41

Figure 4.18: Noisy fringe patterns with different standard deviations of noise. 42

Figure 4.19: Filtered fringe patterns by weighted mean filter. 43

Figure 4.20: Reconstructed objects with the different standard deviations of noise. 44

Figure 4.21: Applying mean filter on the reconstructed objects..... 45

Figure 4.22: The original pyramid object. 46

Figure 4.23: Noisy fringe patterns with different standard deviations of noise. 47

Figure 4.24: Filtered fringe patterns by weighted mean filter 48

Figure 4.25: Reconstructed objects with the different standard deviations of noise. 49

Figure 4.26: Applying mean filter on the reconstructed objects..... 50

Figure 5.1: The system proposed for triangular fringe projection technique. 54

Figure 5.2: Ideal projector VS real projector rays. 55

Figure 5.3: The proposed algorithm steps. 56

Figure 5.4: Triangular fringe patterns generated for projection. 57

Figure 5.5: Image pre-processing steps. 58

www.manaraa.com

Figure 5.6: Cube object form a shadow due to its nature 59

Figure 5.7: proposed algorithm needed steps. 62

Figure 5.8: drawn lines on the base board for angles between camera and projector. ... 63

Figure 5.9: The used setup in the proposed technique. 64

Figure 5.10: Triangular shape with side and top view. 66

Figure 5.11: The two slopes in the same period in triangular fringe pattern. 67

Figure 5.12: Experiment setup for image acquisition. 68

Figure 5.13: Loading and cropping of fringes images. 68

Figure 5.14: Loading and cropping of edges images. 69

Figure 5.15: Fringes image in gray level. 69

Figure 5.16: Edges images in gray level. 69

Figure 5.17: Binarize edges images by thresholding. 70

Figure 5.18: Images after applying the filter. 70

Figure 5.19: One line selection from object image at row 100 71

Figure 5.20: One line selection from reference image at row 100 71

Figure 5.21: Object and reference reconstruction for one line. 72

Figure 5.22: Height distribution line 72

Figure 5.23: Reconstructed object. 73

Figure 5.24: Reconstructed object after calibration. 73

Figure 5.25: Curved paper object and its dimensions. 74

Figure 5.26: Visualization of the curved paper object after the reconstruction process. 75

www.manaraa.com

Figure 6.1: Example of a fixed setup 77

Figure 6.2: A comparison of processing time for the three techniques. 80

Figure 6.3: A comparison in speeding up of triangular relative to saw-tooth. 80

Figure 6.4: the processing time for the used computers and for several computers. 81

Figure 6.5: the speed of the used computer and the speed of several computers. 82

www.manaraa.com

List of Tables

Table **Description** **Page**

Table 4.1: RMSE results for different trials of execution for the semi sphere object with ideal and noisy cases, and the average RMSE results for each case. 51

Table 4.2: RMSE results for different trials of execution for the car roof object with ideal and noisy cases, and the average RMSE results for each case. 52

Table 4.3: RMSE results for different trials of execution for the pyramid object with ideal and noisy cases, and the average RMSE results for each case. 53

Table 5.1: The specifications of Optoma HD141X projector. 64

Table 5.2: The specifications of Samsung wb800f camera. 65

Table 5.3: The specifications of hp ProBook 4540s. 65

Table 6.1: The difference between RMSE results in the ideal case. 78

Table 6.2: Comparing of processing time of different algorithms. 79

www.manaraa.com

List of Abbreviations

Symbol	Description
3D	Three Dimensional
LCD	Liquid Crystal Display
DLP	Digital Light Processing
PC	Personal Computer
FPP	Fringe Pattern Profilometry
CCD	Charge Coupled Device
RMSE	Root Mean Square Error
RGB	Red Green Blue

www.manaraa.com

Abstract

Bawaneh, Mohammad Abdullah. Intensity Based Triangular Fringe Projection Technique for Surface Profilometry Measurements. MSc. Thesis, Yarmouk University, 2017. (Supervisor Dr. Sami Al-Hamdan).

Three Dimensional (3D) shape measurements are used in many applications such as object recognitions, and industrial applications. One of the popular 3D shape measurement techniques is the use of fringe projection methods. In this technique, structured fringe patterns are projected on the targeted object; then the reflected image is captured and analyzed with one of several approaches to reconstruct the 3D shape of that object. In the current study, a new intensity based technique has been developed to resolve some issues with a previous algorithm that uses saw-tooth fringes. The technique relies on fringe projection of triangular fringe patterns. Image enhancement and noise removal techniques are applied on the captured image to enhance the results. The enhanced images are then analyzed to calculate the height distribution of the targeted object using triangulation. In this study, both simulation and real practical experiments are performed to test this new technique. Three different objects with smoothly varying surfaces are tested using the simulation experiments according to two cases: a free noise case and an added noise case, while two other real objects with similar characteristics are used in the practical experiments. Weighted mean filter was tailored for image enhancement of the captured images. The algorithm is able to reconstruct original objects to an acceptable degree, and the root mean square error (RMSE) is relatively low in the simulation experiment. Moreover, a practical experiment has been done. The used setup contains a projector to project triangular fringe patterns, a camera to capture the reflected images, and a PC for generating fringe patterns, and storing and processing the reflected images from the camera. However, the results of reconstruction in the practical case are not very satisfying; it has an RMSE equals to 0.8997. The new algorithm speeds up the execution time by 2.326 relative to the saw-tooth algorithm in the practical case. MATLAB software is used for all programming purposes in this study such as, the experiment simulation, fringe patterns generation …etc.

Keywords: Profilometry, Fringe Patterns, Triangular Fringe Patterns, 3D measurement, Shape Measurement, Fringe Projection

www.manaraa.com

Chapter 1

Introduction

1.1 What is 3D shape measurement

Three Dimensional (3D) shape measurements are used in many fields and applications, such as object recognitions, clothing designs and industrial applications like robot sensing for objects and their dimensions in the space and others. Additionally, they are the core of a design when there is an industrial product which must follow a specific shape and dimensions. For example, several scanning techniques for 3D reconstruction of anatomy can be used, like using 3D computerized images for orthodontic instead of using plaster orthodontic models which are more efficient and easier in taking tooth measurement. Also these images are able to be sent anywhere for research or consultation requests (Adaškevičius and Vasiliauskas, 2015).

Another example of using scanning techniques is the measurements of human body parts. Foot scanning in footwear development applications leads to evolutionary products; particularly for persons who need customized measurements such as players. Figure 1.1 shows foot scanning (Telfer and Woodburn, 2010).

Figure 1.1: 3D image for foot scanning(Telfer and Woodburn, 2010).

www.manaraa.com

3D shape measurement techniques could apply two methods: contact or non-contact methods. In the contact method a physical connection between the measurement tool and the targeted object is to be made. The problem in this method is that it is slow and not possible on some objects such as soft ones, In addition, it may damage some type of objects like lenses for example (Salvi et al., 2010).

In the current study, the focus will be on non-contact methods in which there is no physical connection with the object. Thus it will be more flexible and has no effect on the object. In addition, it is faster and more accurate than the contact method (Chen et al., 2007),(Zhang, 2012).

With respect to non-contact 3D shape measurement techniques, there are two main types: active and passive. Passive 3D shape measurement is used for dynamic objects which vary in location with time. It does not use any kind of radiation. Hence, it requires simple setup (Su and Zhang, 2010), see Figure 1.2.

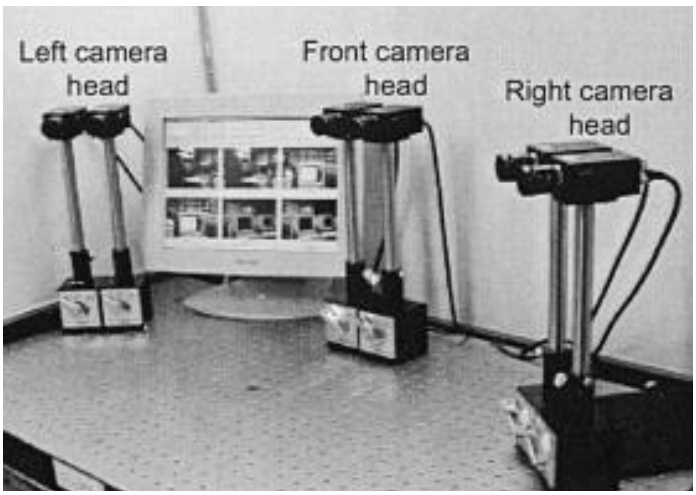

Figure 1.2: Example of multi-camera passive 3D shape measurement system(Muquit and Shibahara, 2006).

On contrary active 3D shape measurement is based on a kind of radiation. It can be classified into two main category: the first one is based on time delay, and the second is

www.manaraa.com

based on triangulation. Time delay is a way to measure the time delay between a projected light beam and the reflected beam from an object under measurements. Since the light beam travels at the speed of light, the time delay from the instant of projecting the beam to the instant of detecting the reflected beam can be used to measure the distance from the point of reflection to the source. Thus, a 3D map can be constructed by scanning the surface of the object. Police speed laser detectors operates on the same principle.

Triangulation uses structured light patterns which are projected on the targeted object to specify the 3D shape (Su and Zhang, 2010). Fringe projection profilometry is a widely used technique; it is a non-contact method for 3D shape measurements of objects. Fringe projection profilometry is based on the projection of a fringe pattern on the surface of the targeted object and the capturing of the reflected image by a camera. This reflected image carries information about the targeted object which can be analysed using different techniques; such as Fourier transform profilometry, spatial phase detection …etc, to compute the surface map (Wu et al., 2013). See Figure 1.3 and 1.4.

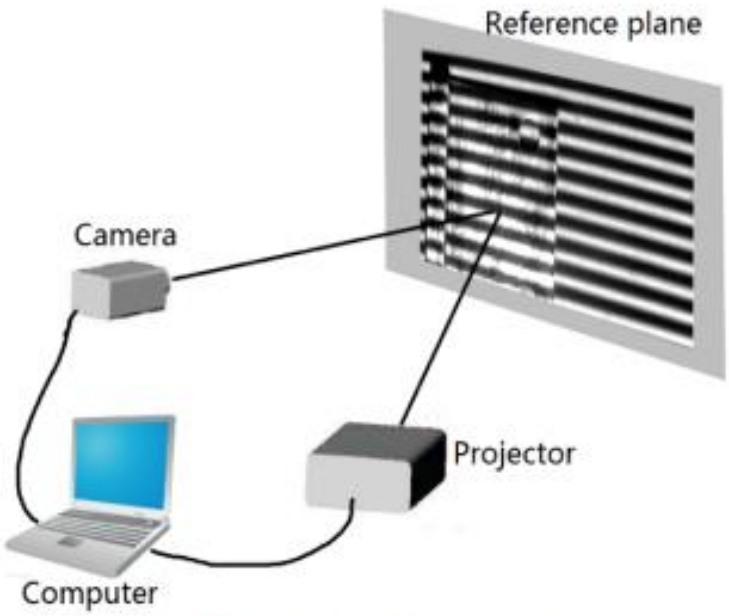

Figure 1.3: Example of an active 3D shape measurement system (Xu et al., 2014).

www.manaraa.com

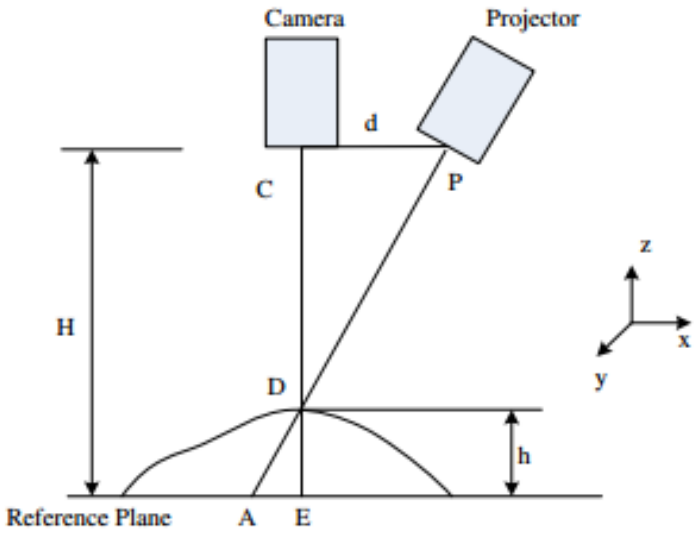

Figure 1.4: Fringe projection profilometry system (Wu et al., 2013).

Fringe patterns are generated by several interferometric techniques such as grating projection system, spatial light modulator, programmable Liquid Crystal Display (LCD) …etc. Digital Light Processing (DLP) and LCD projectors provide flexibility to project different patterns generated by a personal computer (PC) (Gorthi and Rastogi, 2010).

1.2 Fringe Patterns

There is more than one option of fringe patterns, such as sinusoidal and triangular patterns. In this section, some patterns that are used in fringe projection technique will be discussed:

1.2.1 Sinusoidal Fringe Patterns

Sinusoidal patterns are studied mostly, we can generate it by laser interferometer or using computer software to project these patterns on the targeted object. After that the deformed sinusoidal intensity reflected from the surface of an object is used for height calculations (Zhang, 2012). See Figures 1.5 and 1.6.

www.manaraa.com

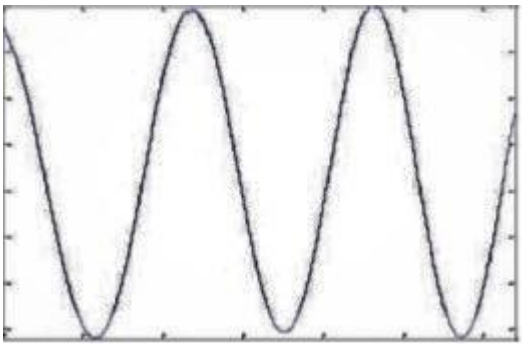

Figure 1.5: One dimensional sinusoidal fringe patterns (Zervas et al., 2011).

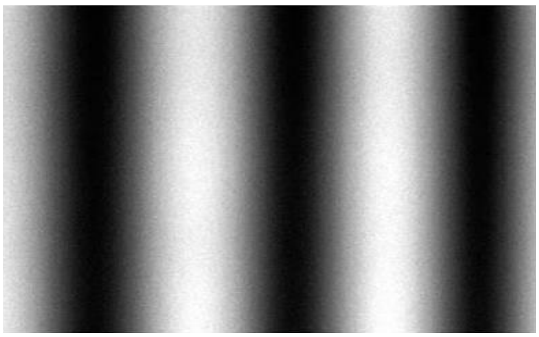

Figure 1.6: Two dimensional Sinusoidal fringe patterns (Zervas et al., 2011).

1.2.2 Binary Patterns

In Binary patterns, there are only two values: 0 which indicates dark and 1 which indicates bright. One of the advantages of these patterns is that these patterns are less effected by noise and many images have to be used. However, resolution is good (Talebi et al., 2013), see Figure 1.7.

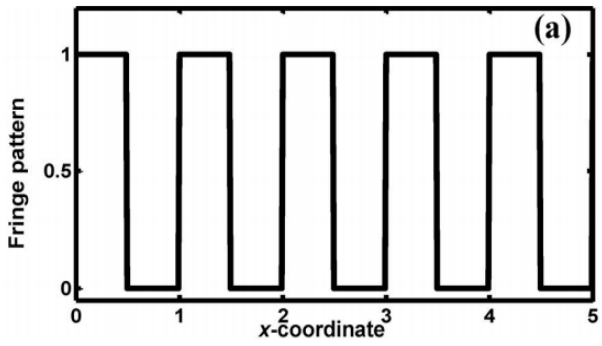

Figure 1.7: One dimensional binary fringe patterns (Ayubi et al., 2010).

www.manaraa.com

1.2.3 Saw Tooth Fringe Patterns

Saw tooth fringe patterns are non sinusoidal, the intensity is increasing (from black to white) until reaching the maximum value and making an abrupt change from white to black. This will be repeated many periods as shown in Figures 1.8, and 1.9 (Al-Hiary, 2015), (Chen et al., 2005).

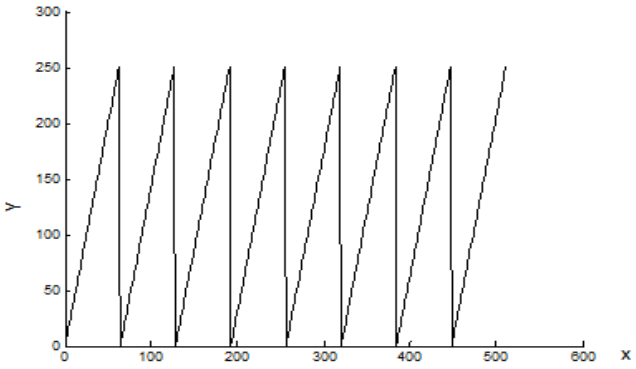

Figure 1.8: One dimensional of saw tooth fringe pattern (Al-Hiary, 2015).

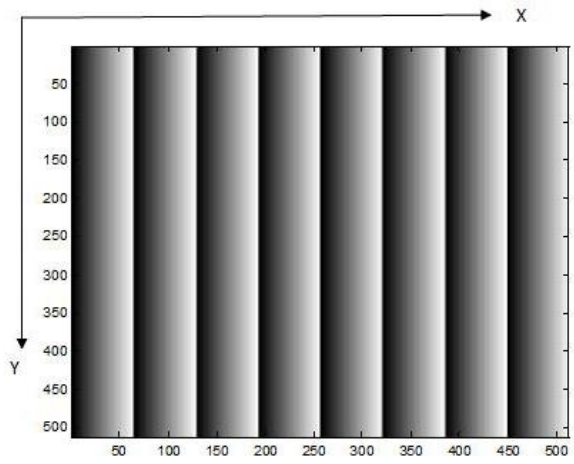

Figure 1.9: Two dimensional of saw tooth fringe pattern (Al-Hiary, 2015).

1.2.4 Triangular Fringe Patterns

These patterns differ from saw tooth fringe patterns. Triangular fringe patterns do not make a sharp drop from white to black. See Figure 1.10 and Figure 1.11 (Cao, 2015).

www.manaraa.com

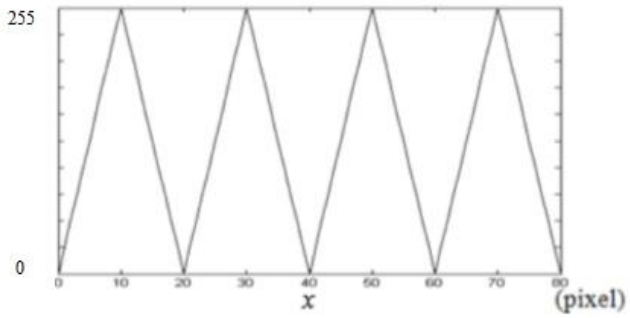

Figure 1.10: One dimensional triangular fringe patterns (Cao, 2015).

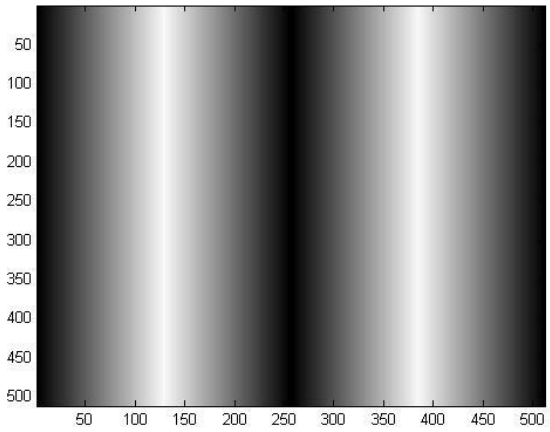

Figure 1.11: Two dimensional triangular fringe patterns.

1.3 Motivation and Problem Statement

3D imaging is a technology that is widely used in many applications and is expanding rapidly. Finding simple and inexpensive techniques for this technology is the main objective of this study. Here, the researcher expects that using triangular fringe projection with intensity based technique has a potential in this industry.

The main objective of the study is to modify the technique presented in Al-Hiary thesis (Al-Hiary, 2015) by changing the shape of the projected fringe pattern from saw-tooth to triangular. This change of shape is expected to enhance results by eliminating the problems of the saw-tooth shape at the fringes boundaries. In saw-tooth fringe patterns the abrupt change of light intensities at the fringe boundaries has caused errors that affected the accuracy and demanded extra computations to reduce their effect. By using

www.manaraa.com

triangular fringe patterns, the change of light intensities at the fringes boundaries is not abrupt; then, the results are expected to be more accurate with less computations.

The problem with saw-tooth fringe pattern is the averaging of border pixels at edges between fringes periods that is inherent in digital cameras. Since this is an abrupt change from white to black at the fringe periods, the pixels at borders do not reflect the actual intensities causing problems in accuracy and requiring extra work to remove such noise. See Figure 1.12, the arrow indicates the pixels with wrong intensity due to the averaging of border pixels at edges problem.

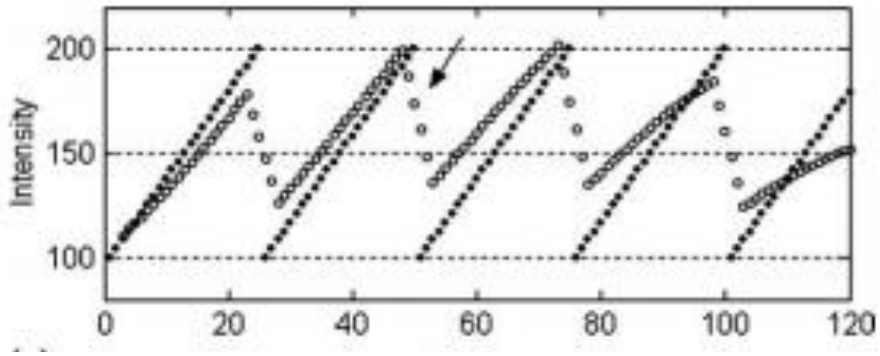

Figure 1.12: Cross sectional line intensity of an object (Chen et al., 2005).

In this study a triangular patterns was used for fringe projection to minimize the error caused by transition from white to black and enhance the performance. A projector and a camera are used to project triangular patterns on the targeted object and to capture the reflected image. This image is analysed and enhanced using image processing techniques.

The main objective of the current study is get rid of the wrong intensities on the edges in the saw-tooth fringe projection technique which caused by the averaging that camera do. This will lead to speed up the system, because the curve fitting computations which needed to correct the intensities values on edges will eliminate.

www.manaraa.com

1.4 Contribution

The proposed algorithm in this study leads to the following contributions:

- Developing a new 3D shape measurement technique that uses a triangular waveform shape for fringes as a better alternative technique to intensity based saw-tooth technique presented by Al-Hiary (2015).
- Developing necessary image enhancement filter that are suitable for our new technique.

1.5 Thesis Organization

The current study contains six chapters. An introduction and a solid literature review on 3D reconstruction of objects are included in chapters 1 and 2. Chapter 3 introduces the methodology and approach of the proposed algorithm. Chapter 4 introduces simulation experiments to verify the correctness of the proposed algorithm. Chapter 5 shows the practical experiments, and the needed steps and techniques to reconstruct 3D objects. Chapter 6 introduces discussion for our work. Finally, conclusion and future work are suggested in chapter 7.

www.manaraa.com

Chapter 2

Literature Review

3D shape measurements have been a hot topic for researchers in recent years. Different techniques discovered and used.

Furukawa and Kawasaki (2003) used a video camera and a laser projector that emits a laser plane not a beam, the laser is connected with LED markers as shown in Figure 2.1 below. The process needs a laser plane beam to be projected on the targeted object producing a stripe on the object surface. The stripe is moved across the object to scan the whole surface while a video camera is recording this stripe. By analysing this video sequence and estimating the parameters of the marker plane; the dimensions of the object are obtained using triangular geometry. Each pixel will take a specific depth in the captured image and is stored in a depth image. The system scans the same pixels more than one time, therefore, the average depth for each pixel is computed to minimize errors. The advantages of this system is that it can be used for parts of shape not for the whole shape; furthermore it is a low cost system.

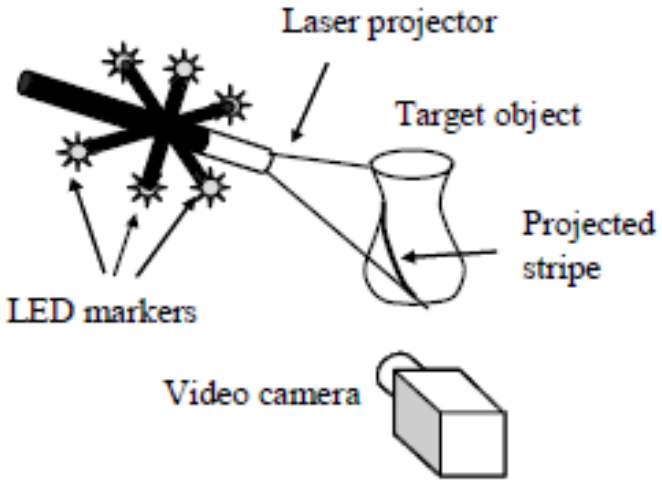

Figure 2.1: Marker attached laser projector-system configuration (Furukawa and Kawasaki, 2003).

www.manaraa.com

Another technology to measure 3D object is the use of time-of-flight 3D camera. It consists of CMOS chip and infrared light source, this source will beam the light on the object and the travel time of this light is measured and converted to depth information. This procedure is done for every pixel in the scene. The user should determine the distance between the camera and a reference plane to determine the depth of a specific point of the object (the point of the reflected infrared light). This scan is done from all viewpoints by rotating the object or by moving the camera around the object, it is a probabilistic multi-scan algorithm, see Figure 2.2. (Cui et al., 2010).

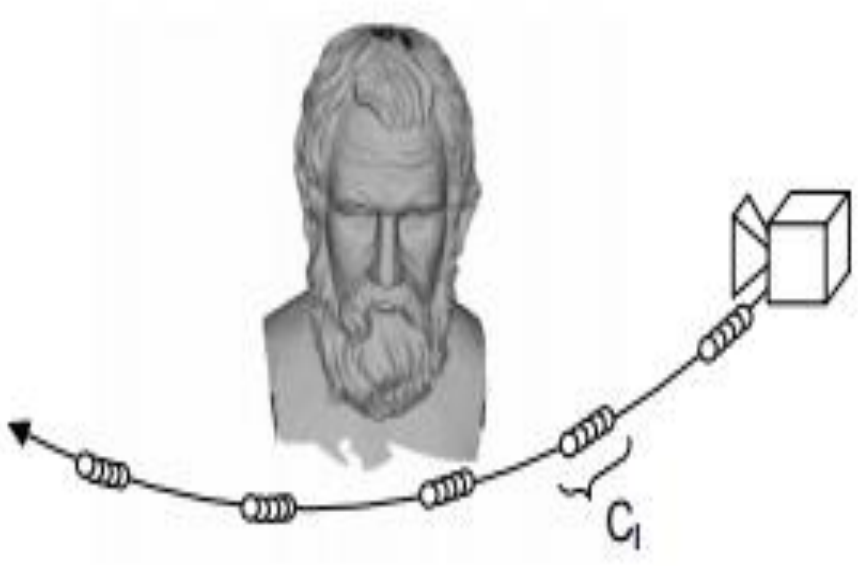

Figure 2.2: A scan from all viewpoints by moving the camera around the object (Cui et al., 2010).

Chen et al. (2013) proposed a new 3D profile measurement system which uses the stereo vision technique. In this system they used multiple cameras which are calibrated to work with each other as a single system. These cameras can be grouped as pairs; each pair of camera works as a stereo vision system. Moreover, each pair will work on a specific part on the targeted object to measure this part based on the principle of triangulation. As a result, the data from each pair will be mapped to the global coordinate system and the 3D targeted object will be extracted. For the experiment setup see Figure 2.3.

www.manaraa.com

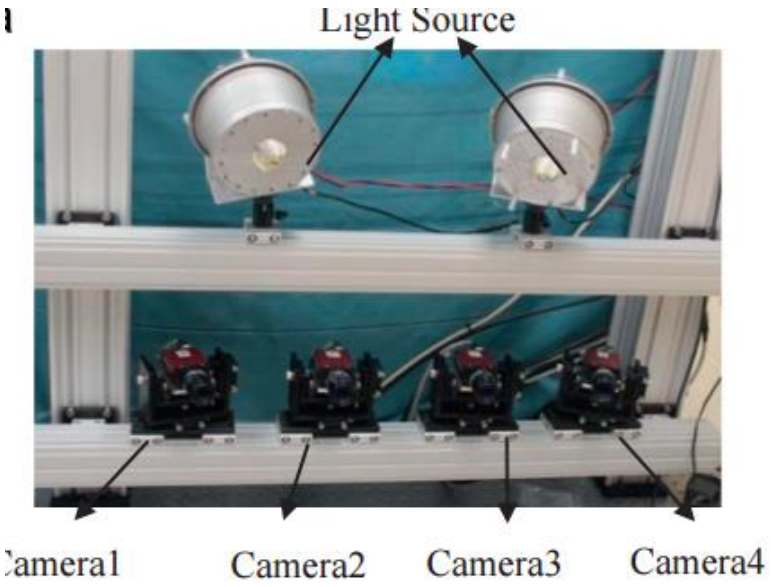

Figure 2.3: The proposed system using four cameras (Chen et al., 2013).

The typical 3D shape measurements use fringe projection techniques and they are summarized by the following major steps: firstly, a structured light pattern is projected on the object surface causing a phase modulation between the object surface and the projected fringe patterns. Secondly, the reflected image is recorded and analyzed to extract phase information, and finally, the height of the surface of the object is computed using the phase information extracted in the second step. Different analysis techniques are used: the Fourier transform is perhaps the most popular spatial based detection algorithms (Takeda and Mutoh, 1983), the phase extracted is unwrapped using different methods, and finally the real heights of the object are computed (Gorthi and Rastogi, 2010).

Chen et al. (2007) combined color encoded stripes and cosinoidal intensity fringes to produce the projected fringe pattern. The height phases on the edges of the strips in the color encoded strips can be obtained and this is used to calculate the heights of the object by triangular geometry. These height phases for each fringe are used to calibrate the relative phase distribution to obtain the absolute height phases.

www.manaraa.com

Wang (2010) proposed in his dissertation to use phase shifting method which uses structured light technique. Phase shifting method provides benefits such as high resolution and accuracy if the user project many patterns on the targeted object. Wang suggested three approaches in phase shifting method in his dissertation. Firstly, after projecting any fringe patterns, Wang proposed edge pattern strategy to achieve maximum signal to noise ratio. Secondly, for fast and reliable reconstruction he developed a novel strategy that used the period information. Thirdly, Wang proposed a hybrid approach for 3D reconstruction; this approach will use structured light with less number of patterns but taking the advantage of using information of phase and modulation data. Wang used two cameras (to take the advantage of multi-view), and DLP projector for the system setup as shown in Figure 2.4.

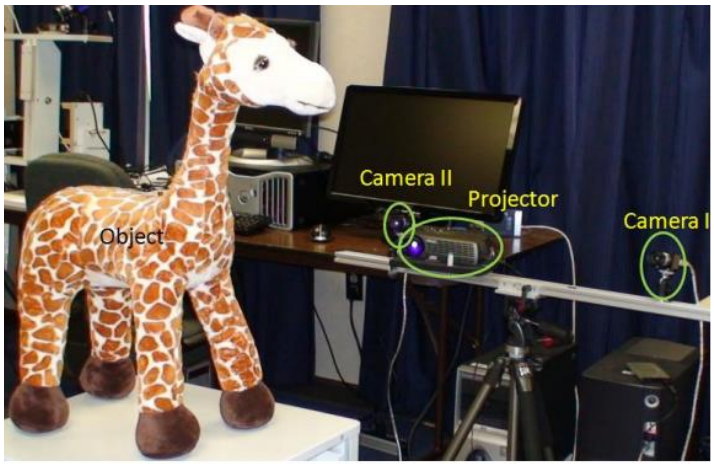

Figure 2.4: The setup for the hybrid system proposed (Wang, 2010).

Another technique is proposed that used Fourier transformation profilometry technique for the dynamic 3D shape measurements as follows: firstly a sinusoidal grating should be projected on the measured object; secondly multiple images are captured by a camera and saved on the computer directly. Then, the data is processed as follows: the Fourier transform is used to obtain image spectra, and then a suitable band pass filter is applied in the frequency domain to get rid of most noise and DC component. Then the inverse

www.manaraa.com

Fourier transform is applied and the wrapped phase information is calculated; finally, phase unwrapping algorithm is applied to generate the unwrapped phase map which is used to reconstruct the heights of the measured object (Su et al., 2001), (Zhang and Su, 2002).

Gong and Zhang (2010) suggested a technique that is a combination of binary structured light and sinusoidal fringe analysis which will achieve high spatial resolution in addition to high temporal resolution. They used a binary gray level (0 and 255), to make the operation of the digital micro mirrors as OFF or ON. A digital micro mirror is a device that achieves precise light switching; it consists of an array of microscopic mirrors and each mirror refers to one pixel in the projected image. The Fourier method is used for 3D shape measurement. They used a camera, Digital Light Processing (DLP) projector and a lens in front of the projector to focus the projected image into a specific area to make sure that the brightness of the projected image is enough for the camera as shown in Figure 2.5.

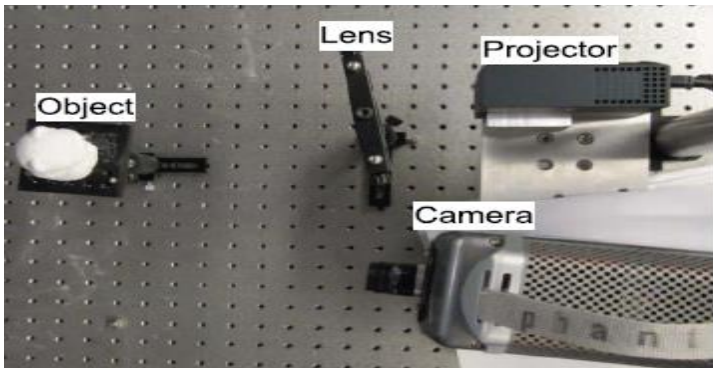

Figure 2.5: Photograph of the test system (Gong and Zhang, 2010).

Fringe image generation by the DLP projector is applied with a specific projection rate; while the exposure time of the camera cannot be shorter than single channel projection time. So, the camera must be synchronized with the DLP projector to capture the image, channel by channel, correctly. Gong and Zhang (2010) used Dell M109S projector which

www.manaraa.com

is inexpensive projector and includes a high speed CMOS camera Phantom V9.1 which captures images with a rate of 2000 Hz in their experiment to verify the performance of the proposed system.

One of the techniques that are used for 3D measurements is to project a fringe pattern on a reference flat plane to determine the correct distribution of the patterns on the flat plane and make it a reference. After that, the pattern is projected onto the object and the reflected image is captured for both: the reference plane and the object. 3D information is found in the difference between the original (flat plane) image and object image and are analyzed by using a mathematical model. On a specific point, the reflected intensity in the reference plane image will be shifted to another point in object image and by using the value of this shift and the triangulation geometry principles the heights of the object points can be calculated. See Figure 2.6 (the intensity reflected from C is the same reflected from D) (Hu et al., 2009), (Hu et al., 2006).

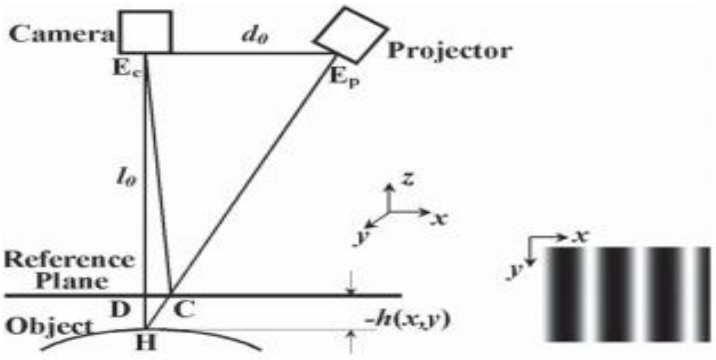

Figure 2.6: Schematic diagram of 3D shape measurement system using fringe patterns technique (Hu et al., 2009).

Cao (Cao, 2015) proposed a new approach in the fringe pattern profilometry (FPP) for 3D profile measurements. He implemented a fringe projection system for his experiment and he proposed to use triangular fringe patterns instead of using sinusoidal patterns due to their limitations which were discovered in previous studies. Moreover, he solved the

www.manaraa.com

problem of the shift unwrapping by proposing reliability guided and multiple wavelength algorithms. Thus, he found a method for 3D profile measurements by projecting two wavelengths of triangular fringe patterns, see Figure 2.7.

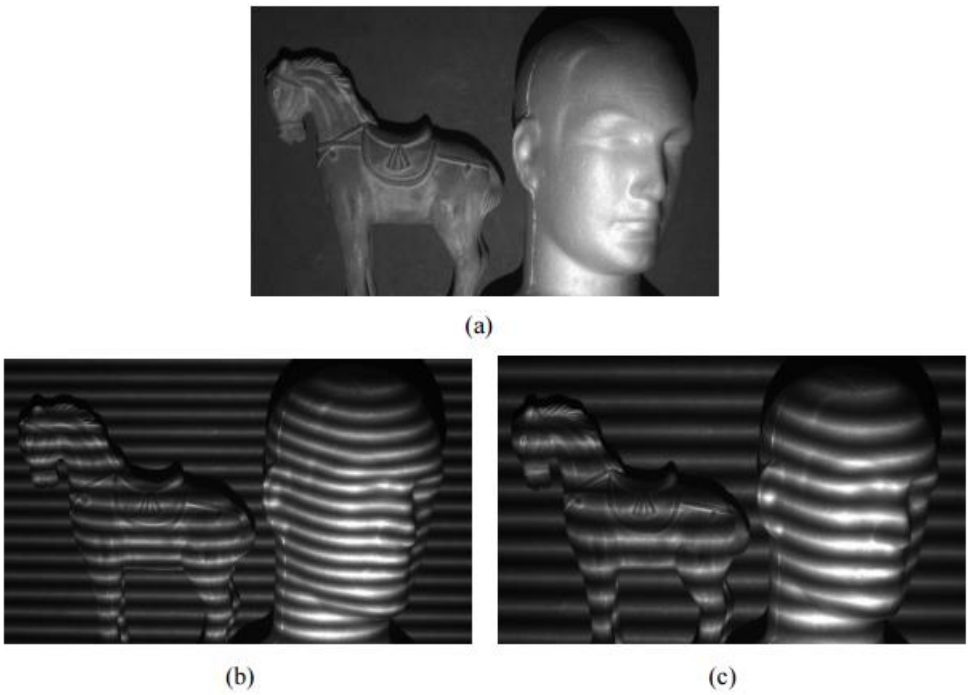

Figure 2.7: Triangular patterns projection experiments with two selected wavelength: (a) targeted objects, (b) and (c): fringe projection with different wavelength (Cao, 2015).

Al-Hiary (2015) proposed a new technique for 3D profilometry. This technique used DLP projector and a charge coupled device (CCD) camera in addition to PC for computations and analysis of captured image (see Figure 2.8). She used saw-tooth fringe patterns to project on the target (Figure 2.9). The user need to project these patterns to reference flat plane and capture the reflected image. Then, the user should project the same patterns on the targeted object. After applying the suitable technique for noise removal on the captured images; the object depth information is calculated by triangulation. The problem in this technique is the averaging of borders pixels at edges between fringe periods that is inherited in digital cameras. When the transition from one

www.manaraa.com

period to the next period happens, the borders pixels do not show the actual intensities due to the camera averaging and this causes problems in accuracy.

Figure 2.8: Experiment setup of saw tooth projection (Al-Hiary, 2015).

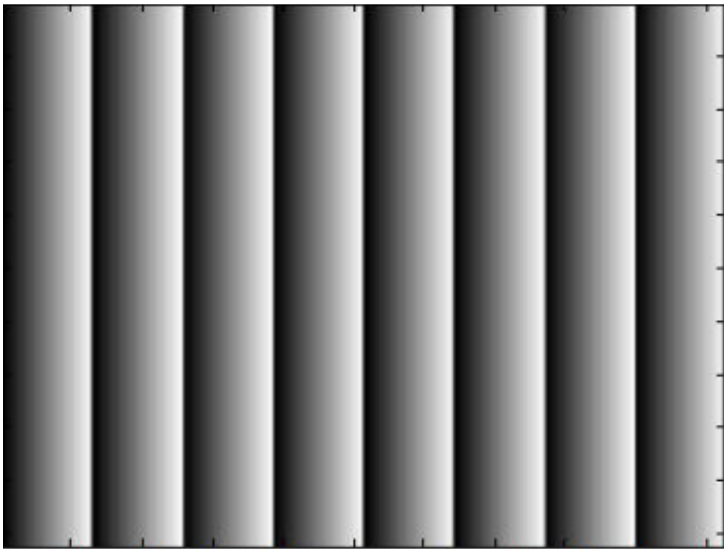

Figure 2.9: Saw tooth fringe patterns (Al-Hiary, 2015).

www.manaraa.com

Chapter 3

Methodology and Approach

This chapter presents the triangular fringe patterns specifications and their advantages over saw-tooth fringe patterns, patterns generation, in addition to a simulation of triangular fringe patterns technique to verify the correctness of the proposed technique.

3.1 Triangular Fringe Generation and Projection

The triangular fringe patterns are periodic patterns which are increased gradually from minimum value to maximum value (from black to white) and back again to decrease gradually to the minimum value in one period (from white to black). It is named triangular due to its wave shape which is similar to triangle, see Figure 3.1 which shows an example of triangular wave form with amplitude of 250 and period of 64.

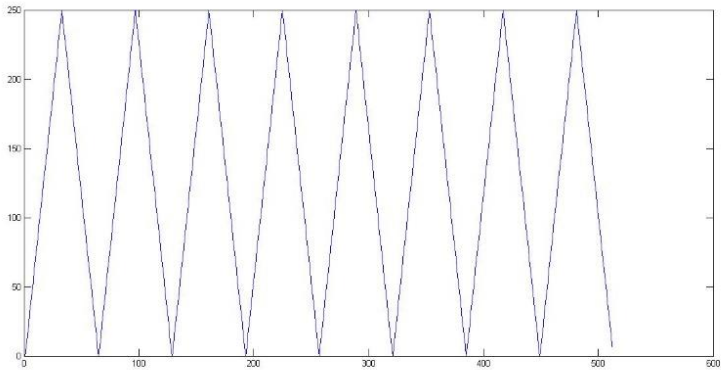

Figure 3.1: Triangular wave form, amplitude = 250, period =64.

The intensity of triangular fringe patterns can be expressed in the following equations (Cao et al., 2014):

$$S(x) = \frac{2a}{To}\, x, \qquad when\ 0 \ \leq\ x \ \leq \frac{1}{2}\, To \tag{1}$$

www.manaraa.com

$$S(x) = 2a\left(1 - \frac{x}{To}\right), \qquad when\ \frac{1}{2}To \leq x \leq To \tag{2}$$

Where (a) is the amplitude, and (To) is the period of the fringe.

Triangular fringe patterns are generated using MATLAB software in gray color with intensity between (0) and (255) (in general) to project these patterns later to the measured objects. See Figure 3.2 which presents an example of triangular fringe patterns generated by MATLAB software, these patterns have an amplitude of 250 and period of 128 pixel.

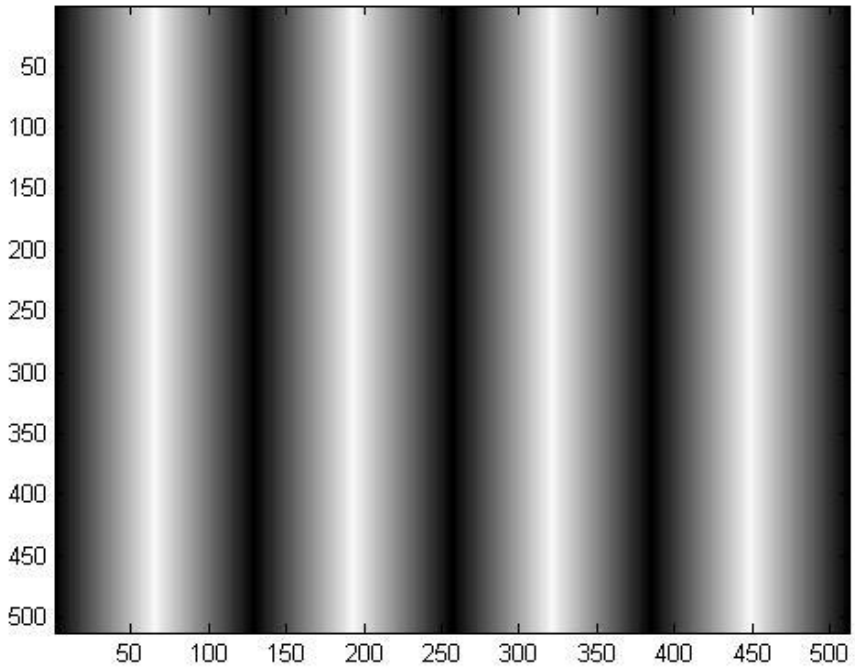

Figure 3.2: Triangular fringe patterns, amplitude = 250, period =128.

3.2 The Selection of Triangular Fringe Patterns

The triangular fringe patterns have an advantage over the saw-tooth fringe patterns. The saw-tooth fringe patterns suffer from the abrupt change from white to black on boundaries (the end of all periods) which leads to make distortions and intensity averaging for pixels on boundaries which are inherited by digital cameras and the defocusing of the digital

www.manaraa.com

projectors. This abrupt change makes the pixels on boundaries not to reflect the actual intensity which requires extra works and computations to decrease its effect on the accuracy of measurement. Since, triangular fringe patterns do not suffer from the abrupt change of intensity; the computations will be less and the accuracy will be better.

Figures 3.3 and 3.4 show the difference between saw-tooth fringe patterns which have the abrupt change of intensity and triangular fringe patterns.

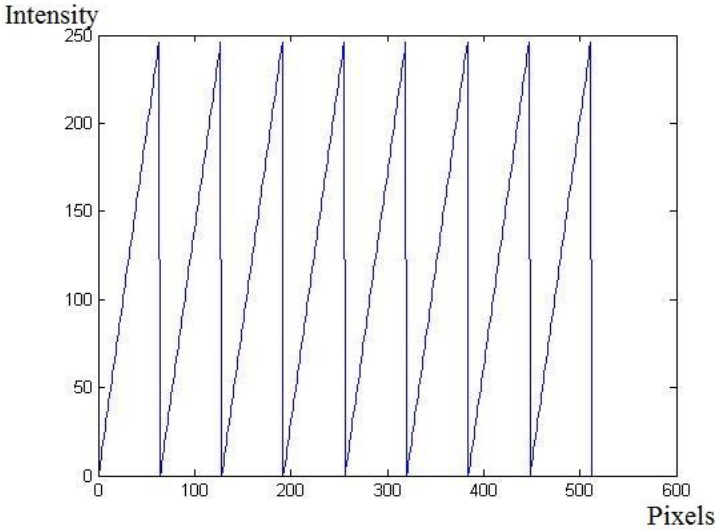

Figure 3.3: One line selection for saw-tooth fringe patterns with amplitude of 250 and period of 64.

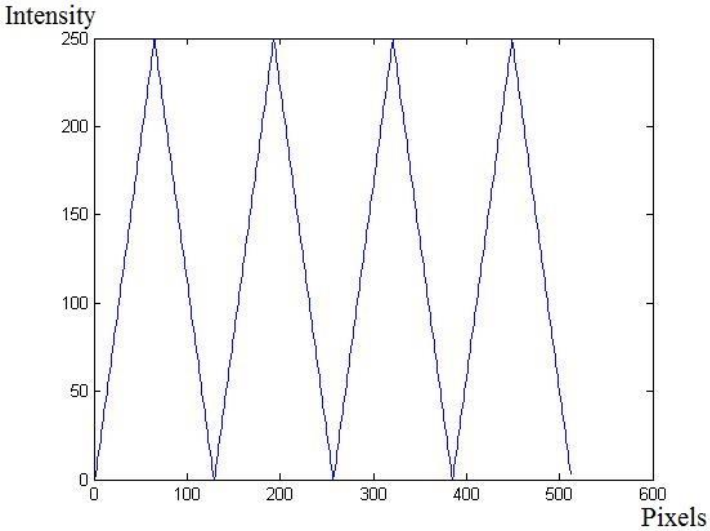

Figure 3.4: One line selection for triangular fringe patterns with amplitude of 250 and period of 128.

www.manaraa.com

Cao (2015) used a testing image that has just two levels of intensity (white and black) to illustrate the abrupt change problem in the practical field as shown in Figure 3.5.

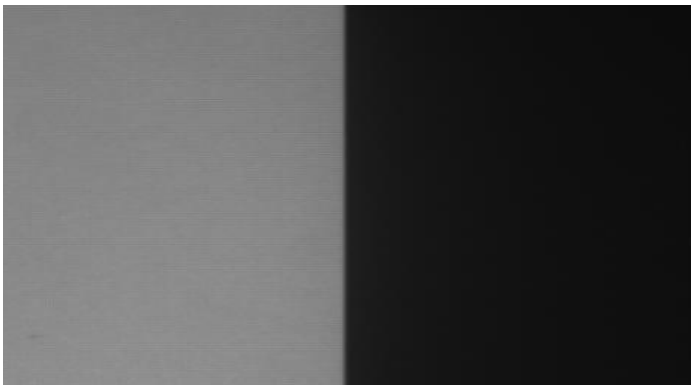

Figure 3.5: Tested image with two intensity levels (Cao, 2015).

Theoretically, by taking one line of this image, it should have a wave that consists of only two values and should make an abrupt change when moving from white to black as shown in Figure 3.6.

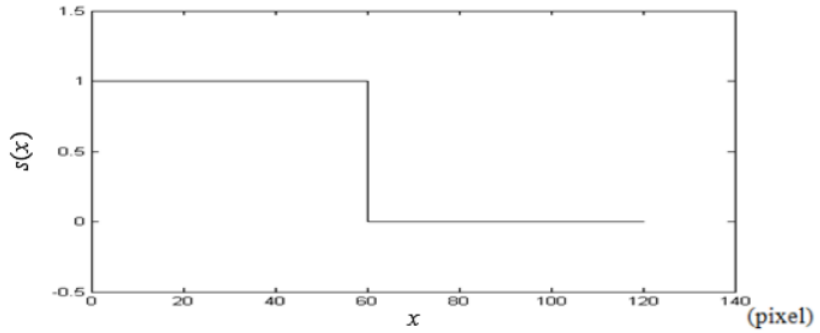

Figure 3.6: Intensity data of white and black image in theory (Cao, 2015).

In real and practical fields, Cao found that after projection and capturing this image; the one line cross sectional had a distortion on the place of change from white to black. As a result of this, it did not make an abrupt change as expected and it did not reflect the real intensity of pixels on this boundary. This what happened in the saw-tooth fringe patterns on all boundaries. See Figure 3.7.

www.manaraa.com

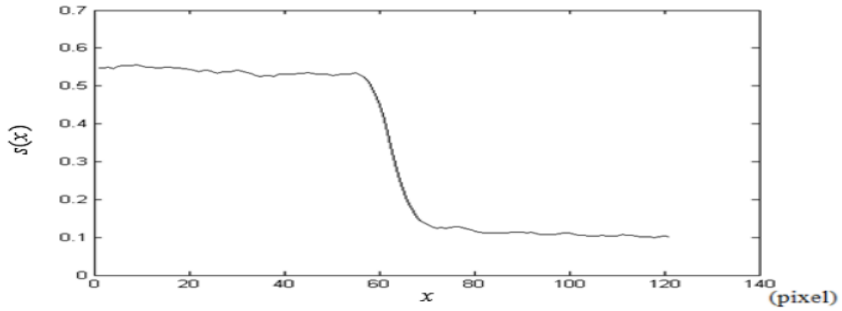

Figure 3.7: One line cross sectional of the captured image (Cao, 2015).

Hence, triangular fringe patterns are used as a new technique in this study; because it does not suffer from sharp drop and hence will avoid the distortion.

3.3 Mathematical Derivation of Heights

By triangulation, we can find a relationship between the difference in height within two points and the difference in light intensity at those two points. So, the difference in height will be calculated from the intensity values of the reflected image by one of the two relations in equation (10) and equation (18) which can be proved by triangulation. For the first have of the period see Figure 3.8.

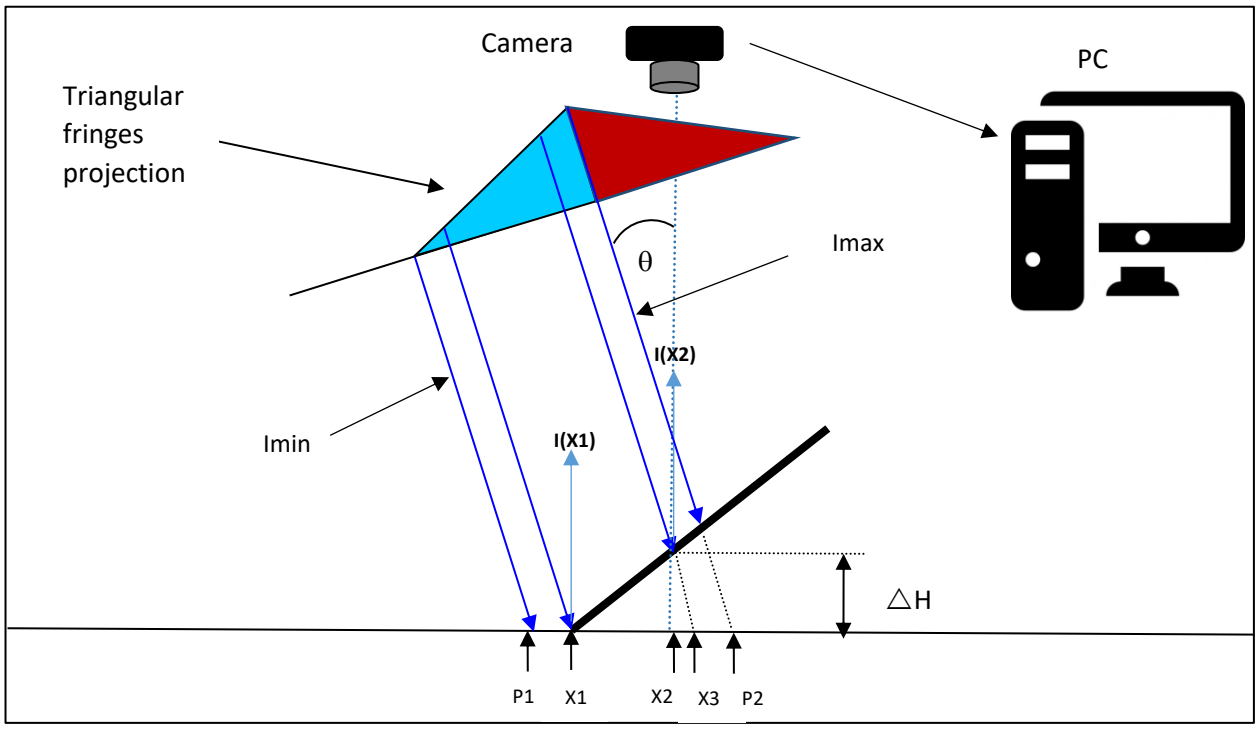

Figure 3.8: Schematic diagram for representation of ΔH (first half of the period).

www.manaraa.com

Imax, Imin, P2, and P1 represent the parameters of the reflected fringe patterns from a flat surface.

The slope of the first half of the fringe pattern (A1) can be written as:

$$A1 = (Imax - Imin)/(P2 - P1) \quad (3)$$

Where (P2 – P1) is the period of the first half of a fringe cycle.

As shown in the above Figure; the reflected light intensity from X2 is the same as the reflected light intensity from X3. This happens if the object is removed.

Thus, the below relation is found:

$$I(x2) - I(x1) = A1 * (x3 - x1) \quad (4)$$

From Figure 3.8:

$$Tan(\theta) = (x3 - x2)/\Delta H \quad (5)$$

Where (θ) is the angle between projector and camera, and ΔH is the difference in height between two points.

So, X3 can be written as:

$$x3 = x2 + \tan(\theta) * \Delta H \quad (6)$$

As a result of combining the relations (4) and (6), the following is found:

www.manaraa.com

$$I(x2) - I(x1) = A1 * (x2 + \tan(\theta) * \Delta H - x1) \quad (7)$$

Let:

$$\Delta I = I(x2) - I\ (x1)$$

$$\Delta x = x2 - x1$$

Then:

$$\Delta I = A1 * (\Delta x + \tan(\theta) * \Delta H) \quad (8)$$

So:

$$\Delta H = \frac{1}{\tan(\theta)} * (\frac{\Delta I}{A1} - \Delta x) \quad (9)$$

Let:

$$\beta = \frac{1}{\tan(\theta)}$$

$$\alpha 1 = \frac{1}{A1}$$

Then:

$$\Delta H = \beta * (\alpha 1 * \Delta I - \Delta x) \quad (10)$$

www.manaraa.com

For the second half of the fringe period see Figure 3.9.

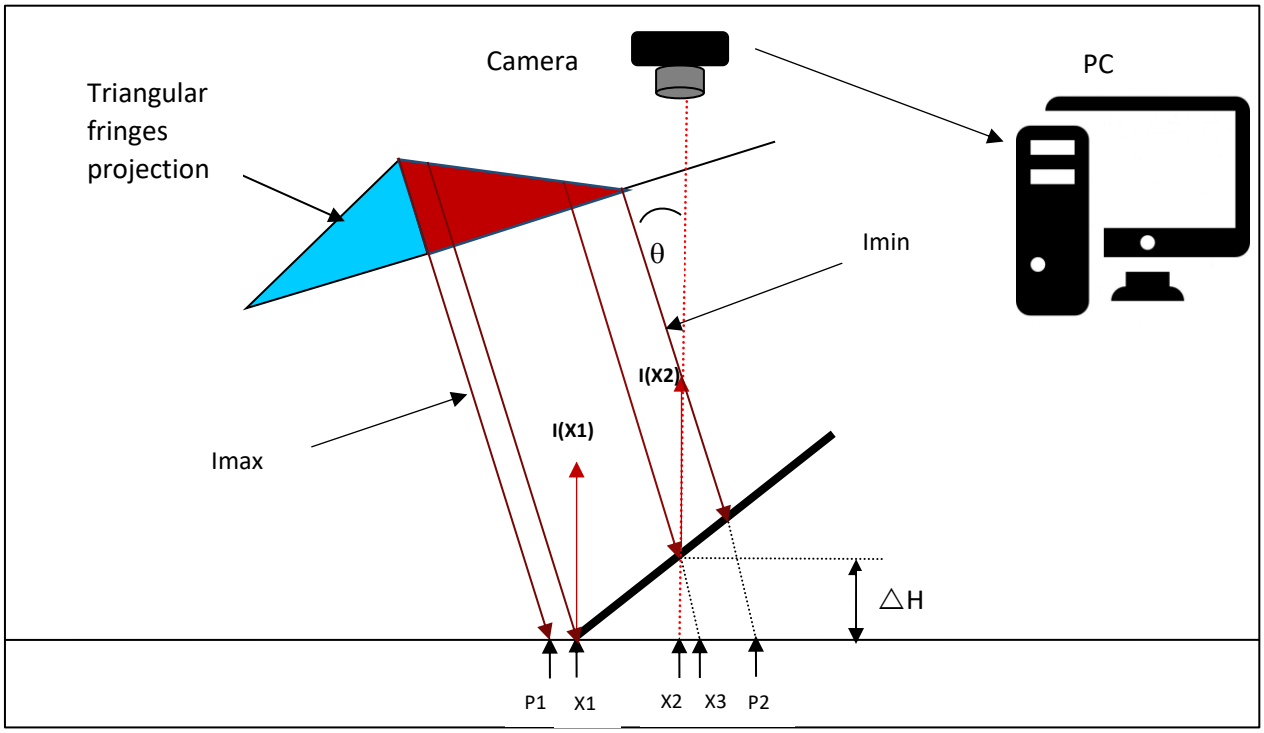

Figure 3.9: Schematic diagram for representation of ΔH (second half of the period).

Imax, Imin, P2, and P1 represent the parameters of the reflected fringe patterns from a flat surface.

The slope of the second half of fringe patterns (A2) can be written as:

$$A2 = (Imin - Imax)/\,(P2 - P1) \tag{11}$$

Where (P2 - P1) is the period of the second half of a fringe cycle.

As shown in Figure 3.9 the reflected light intensity from X2 is the same as the reflected light intensity from X3. This happens if the object is removed.

Thus, the below relation is found:

$$I(x1) - I(x2) = A2 * (\,x1 - x3) \tag{12}$$

www.manaraa.com

From Figure 3.9:

$$Tan(\theta) = (x3 - x2)/\ \Delta H \tag{13}$$

So x3 can be written as:

$$x3 = x2 + \tan(\theta) * \ \Delta H \tag{14}$$

As a result of combining the relations (12) and (14), the following is found:

$$I(x1) - I(x2) = A2 * (x1 - x2 - \tan(\theta) * \ \Delta H) \tag{15}$$

Let:

$$\Delta I = I(x2) - I(x1)$$

$$\Delta x = x2 - x1$$

Then:

$$\Delta I = A2 * (\Delta x + \tan(\theta) * \ \Delta H) \tag{16}$$

So:

$$\Delta H = \frac{1}{\tan(\theta)} * (\frac{\Delta I}{A2} - \ \Delta x) \tag{17}$$

Let:

$$\beta = \frac{1}{\tan(\theta)}$$

www.manaraa.com

$$\alpha 2 = \frac{1}{A2}$$

Then:

$$\Delta H = \beta * (\alpha 2 * \Delta I - \Delta x) \quad (18)$$

Hence, the same equation in the first and the second half of the fringe period is used to calculate height differences but with different slope value which depends on the rising or decreasing half. A1 (in the first half) = -A2 (in the second half).

In this study, this equation has been used to calculate the height of every pixel in the captured image starting from left to right depending on the changing of intensity for each pixel and its previous pixel until reaching the final pixel in the line and then repeating these calculations in similar way to all lines. The heights of all pixels in the image are calculated and the object is reconstructed.

www.manaraa.com

Chapter 4

Simulation

In this chapter, the simulation results are presented for both the ideal and non-ideal cases. Ideal cases are the ones with no noise except the error caused by rounding errors in computer calculation. The non-ideal case is the ones in which noise is added to the fringe patterns image. In this study, three objects simulation are presented. Semi-sphere, car roof, and pyramid objects. These objects was presented and coded by (Al-Hamdan and Hamad, 2008), so we use some code helping for generate these objects for making our simulation of the proposed algorithm on them.

4.1 Simulation with Ideal Conditions

4.1.1 Simulation of Semi-Sphere Object

To verify the correctness of the new technique of the current study; semi sphere object was simulated by using MATLAB software. The semi-sphere surface has maximum height of 75 pixels. A corresponding fringe patterns was generated using relations (8) and (16) with maximum intensity of 222 and minimum intensity of 30, period of 32 pixels, and angle of projection of 15 degrees. After generation of the corresponding triangular fringe patterns, heights calculated by calculating the difference in heights between adjacent pixels using equations (10) and (18). Ideal conditions were assumed here. Figure 4.1 shows the simulated semi sphere object. Figure 4.2 shows the corresponding triangular fringe patterns. Figure 4.3 shows the reconstructed object.

www.manaraa.com

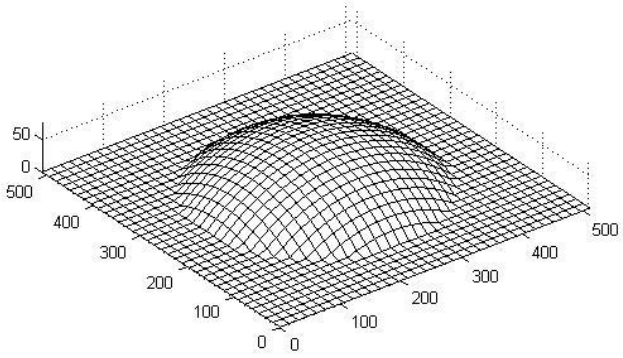

Figure 4.1: The simulated semi sphere object.

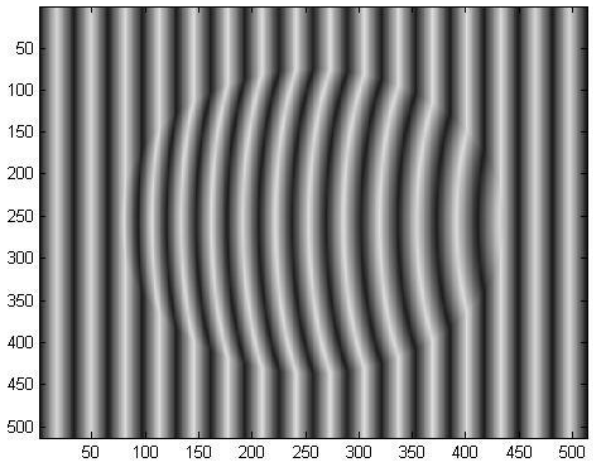

Figure 4.2: The corresponding triangular fringe patterns.

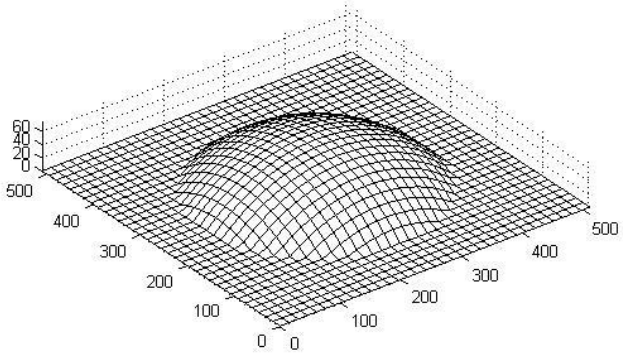

Figure 4.3: The reconstructed object.

www.manaraa.com

The new technique was very successful in reconstructing objects. The result was tested by subtract the line 256 of the simulated object from the line 256 of the reconstructed object to see the difference in heights in the middle line between simulated object and reconstructed object which represents the error in the used technique. And it is found that the maximum absolute error was around 0.3 pixel; this error is caused by rounding errors in computer calculations by relations (8) and (16); since the heights of the original objects are analog and the results of corresponding intensities are rounded to integers to simulate the practical experiment. See Figure 4.4.

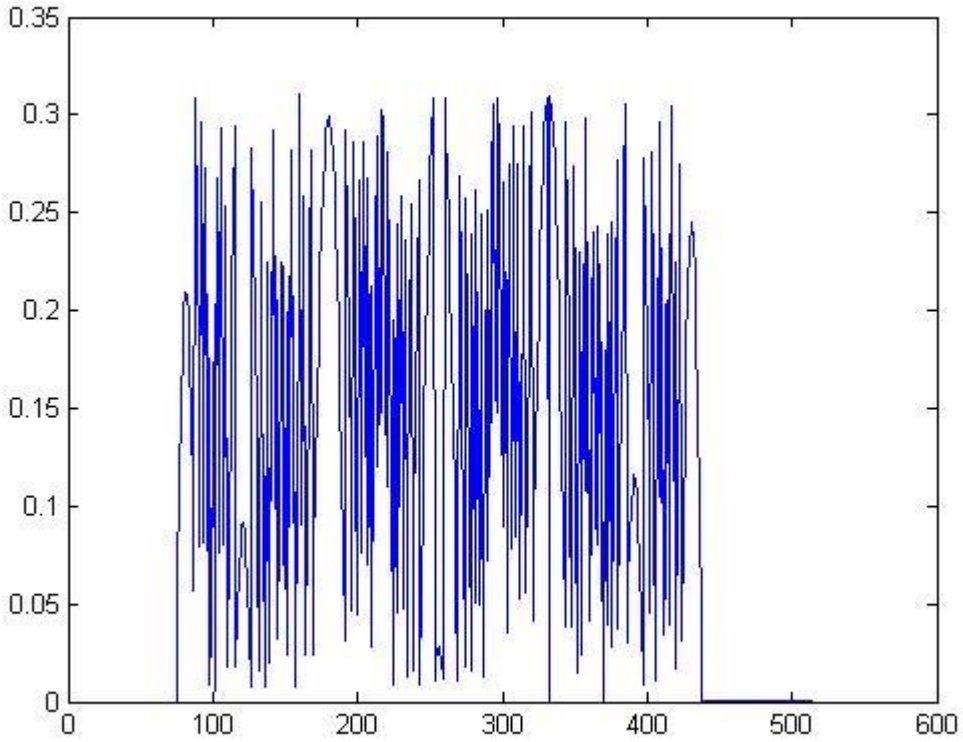

Figure 4.4: The absolute error of the simulation in the mid line of the object.

For describing the average error in the proposed algorithm; one of the most common methods for measuring the average error was used which is the root mean square error (RMSE) (Willmott and Matsuura, 2005), RMSE can be written as:

www.manaraa.com

$$RMSE = \sqrt{\frac{\sum_{i=1}^{n} | e_i|^2}{n}} \quad (19)$$

So, the root mean square error in the middle line in the previous experiment was calculated and it was 0.1547 pixel.

4.1.2 Simulation of Car Roof Object

The second used object is the car roof object with maximum height of 100. A triangular fringe patterns with maximum intensity of 222, minimum intensity of 30, period of 32; in addition to an angle of projection of 15 were used to simulate the projection. See Figure 4.5 to 4.7.

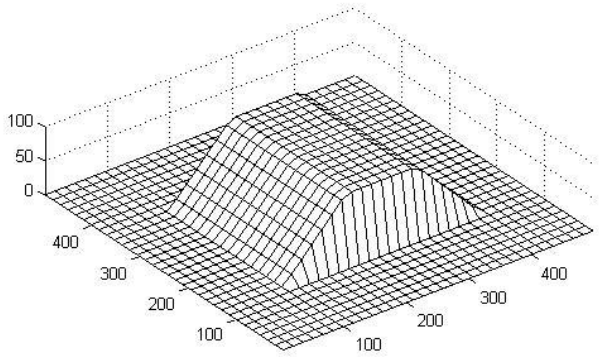

Figure 4.5: The simulated car roof object.

www.manaraa.com

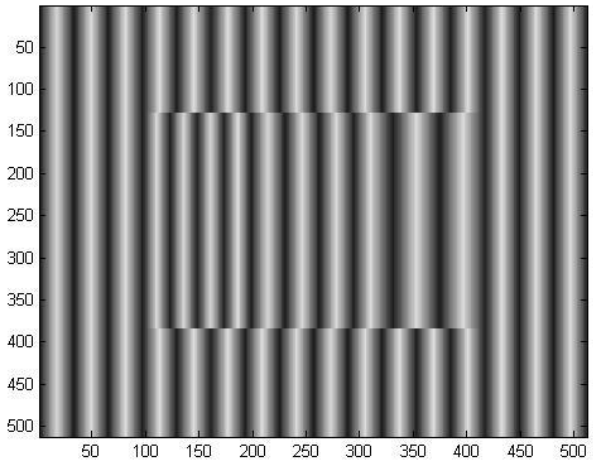

Figure 4.6: The corresponding triangular fringe patterns.

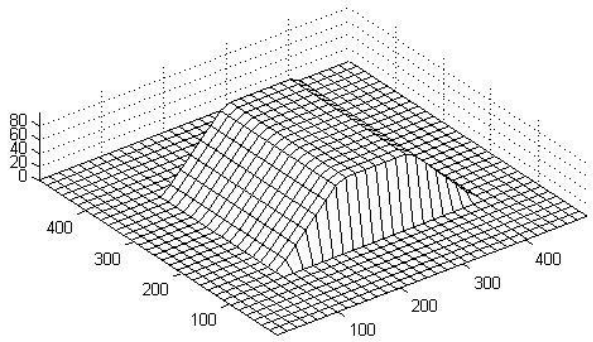

Figure 4.7: The reconstructed object.

4.1.3 Simulation of Pyramid object

The third used object is the pyramid object with maximum height of 60. A triangular fringe patterns with maximum intensity of 222, minimum intensity of 30, period of 32; in addition to an angle of projection of 15 were used to simulate the projection. See Figure 4.8 to 4.10.

www.manaraa.com

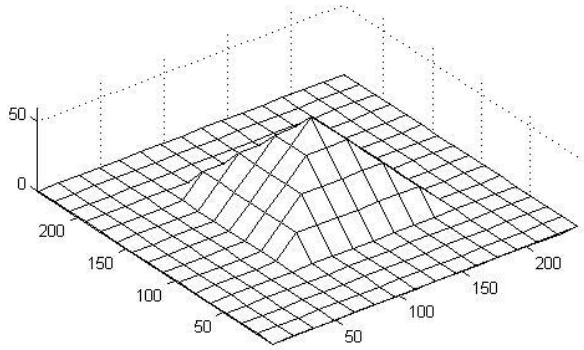

Figure 4.8: The original pyramid object.

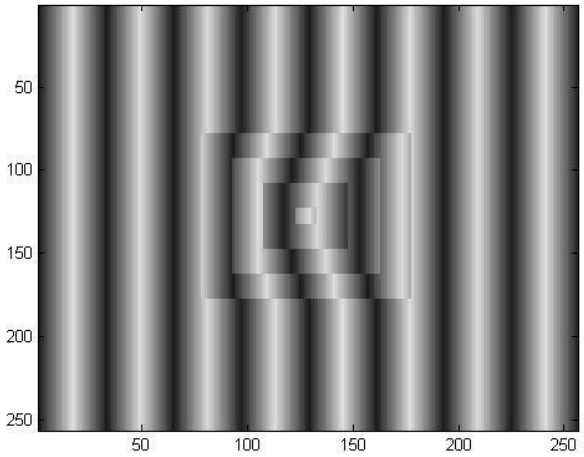

Figure 4.9: The corresponding fringe patterns.

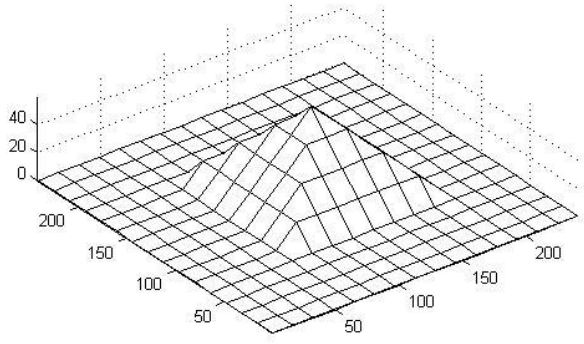

Figure 4.10: The reconstructed object.

www.manaraa.com

4.2 Simulation with an Added Random Noise

In real life and practical experiments, there are many problems causing a not ideal reconstruction. Such as the noise which leads to capture noisy fringe patterns image, so to test the robustness of this algorithm; this problem was simulated by adding random noise to the fringe patterns generated with 0 mean and different standard deviation values (0.1, 0.5, 1, 2, and 5) (Berginc and Jouffroy, 2009), then a special filter was used to enhance the fringe image for illustrating the method of enhancement images that should be used in the practical experiment.

Mean filter is used to enhance the image to make it more smooth. However, in this study if mean filter is used, the values of intensity on the edges of fringe patterns period will be very smooth and their actual effect in the object reconstruction will be lost. Hence, a special filter was made to save intensity values on edges from averaging and losing their actual effect.

The special filter is 5 X 5 filter. To illustrate how it works, see Figure 4.11:

$\frac{1}{36}$	$\frac{1}{36}$	$\frac{1}{36}$	$\frac{1}{36}$	$\frac{1}{36}$
$\frac{1}{36}$	$\frac{2}{36}$	$\frac{2}{36}$	$\frac{2}{36}$	$\frac{1}{36}$
$\frac{1}{36}$	$\frac{2}{36}$	$\frac{4}{36}$	$\frac{2}{36}$	$\frac{1}{36}$
$\frac{1}{36}$	$\frac{2}{36}$	$\frac{2}{36}$	$\frac{2}{36}$	$\frac{1}{36}$
$\frac{1}{36}$	$\frac{1}{36}$	$\frac{1}{36}$	$\frac{1}{36}$	$\frac{1}{36}$

Figure 4.11: A 5 X 5 window of the special filter and the weights for every pixel

www.manaraa.com

Every pixel has different weight; the desired pixel to filter has a weight of 4, the nearest pixels to the desired pixel (the 8 neighborhood) have a weight of 2, and finally the farthest ones have the less weight which is 1. The mean value of these pixels is computed with considering their weights and the result will be the new value of the desired pixel. Equation 20 illustrates the filter computations.

$$New_Value = \frac{\sum_{i=1}^{25}(intensity\ value\ of\ the\ pixel) * (weight\ of\ pixel)}{\sum_{i=1}^{25}(weight\ of\ pixel)} \quad (20)$$

This special filter keeps the intensity values of edges appropriate enough to make their actual effect in the reconstruction process.

As mentioned before, for testing the robustness of this method, a random noise was added to the fringe patterns generated and the special weighted mean filter was applied on the noisy fringe patterns to enhance the image to illustrate the method of image enhancement that should be used in the practical experiment. Moreover, another 5 X 5 mean filter is applied on the reconstructed object after the reconstruction process to enhance the result. These are applied for the three objects.

4.2.1 Simulation of Semi-Sphere with an Added Noise

For the semi sphere object, the same height as the ideal case, the same fringe period, the same maximum and minimum intensities, and the same angle of projection are used. A random noise with five distributions was added, all of them with 0 mean but with different standard deviation values (0.1, 0.5, 1, 2, and 5). The results of this simulation is shown in Figures 4.12 to 4.16 which indicate that the method of this study is robust.

www.manaraa.com

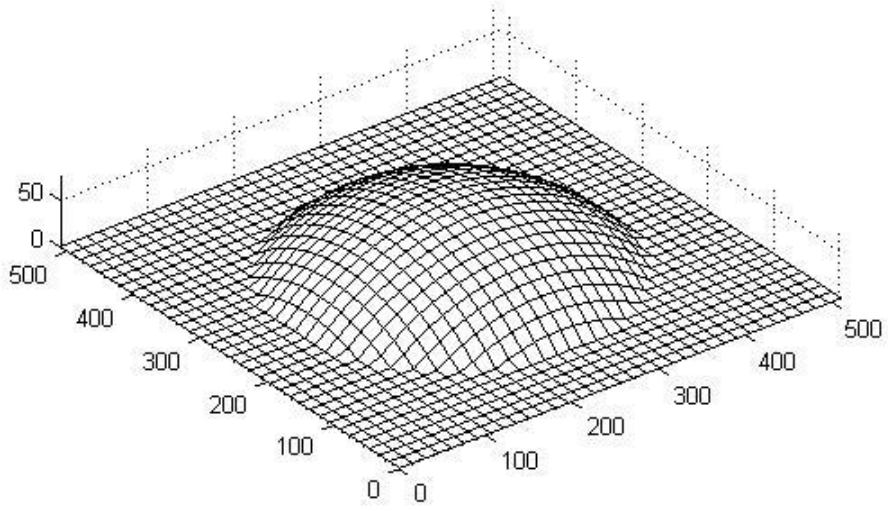

Figure 4.12: The original object.

www.manaraa.com

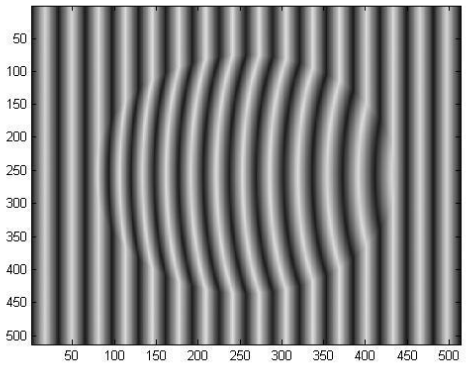

a) $\sigma = 0.1$

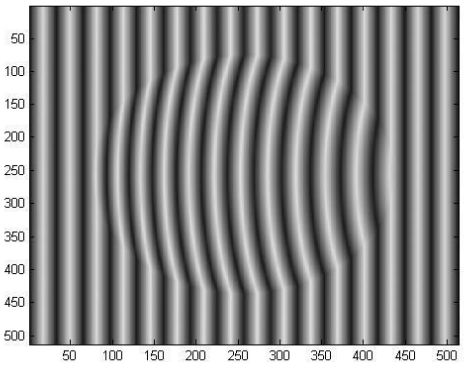

b) $\sigma = 0.5$

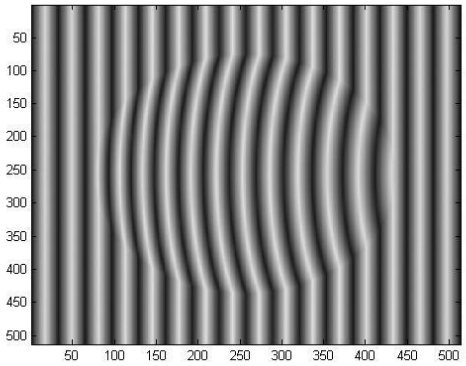

c) $\sigma = 1$

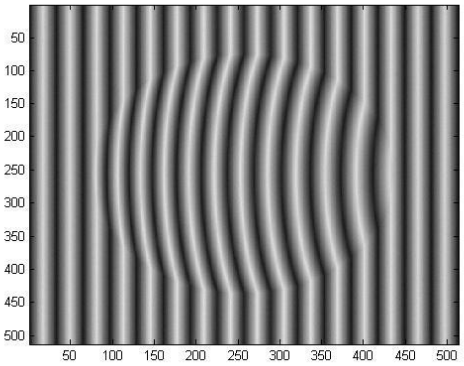

d) $\sigma = 2$

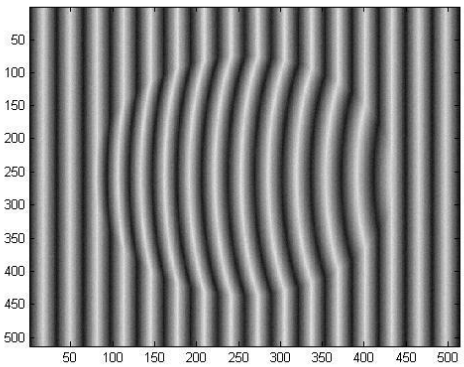

e) $\sigma = 5$

Figure 4.13: Noisy fringe patterns with different standard deviations of noise.

www.manaraa.com

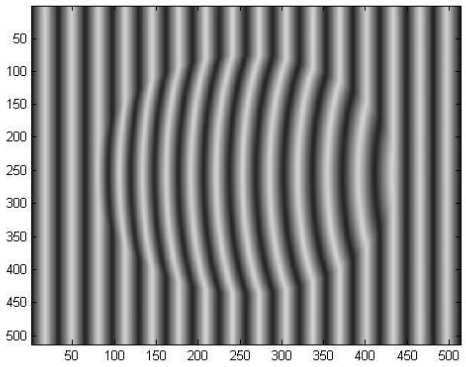

a) $\sigma = 0.1$

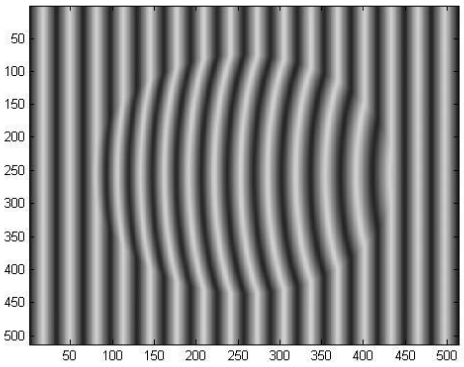

b) $\sigma = 0.5$

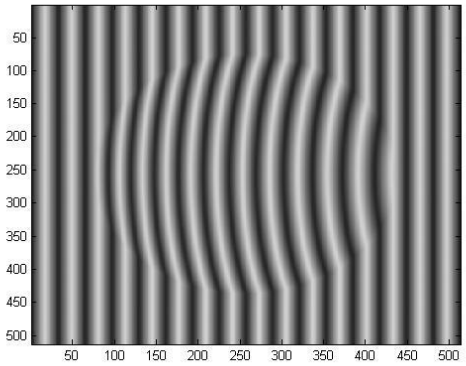

c) $\sigma = 1$

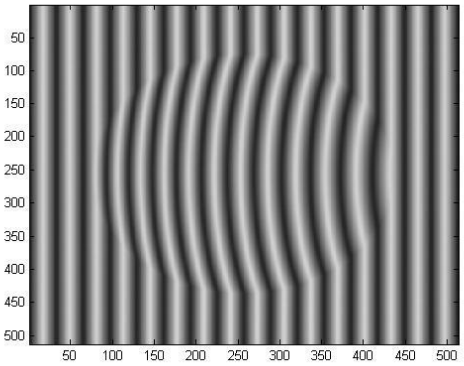

d) $\sigma = 2$

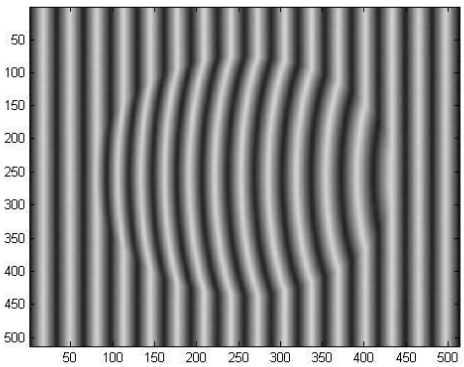

e) $\sigma = 5$

Figure 4.14: Filtered fringe patterns by weighted mean filter with the different standard deviations of noise.

www.manaraa.com

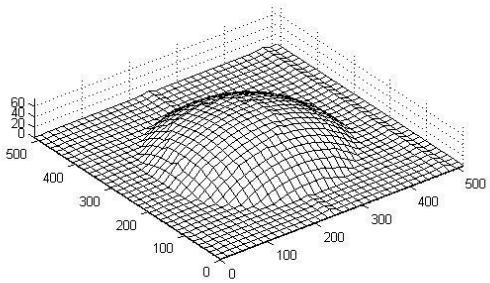

a) $\sigma = 0.1$

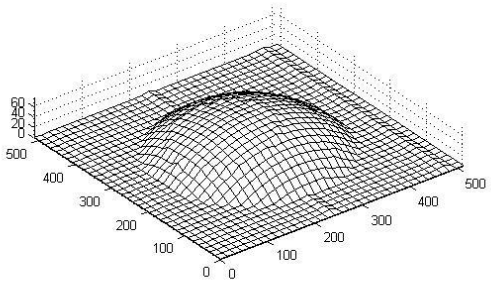

b) $\sigma = 0.5$

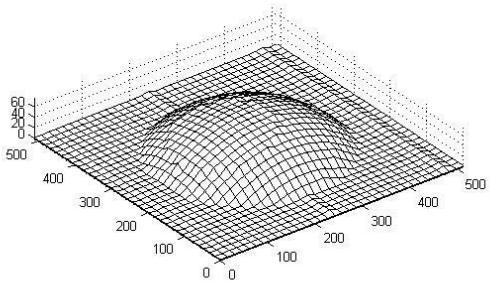

c) $\sigma = 1$

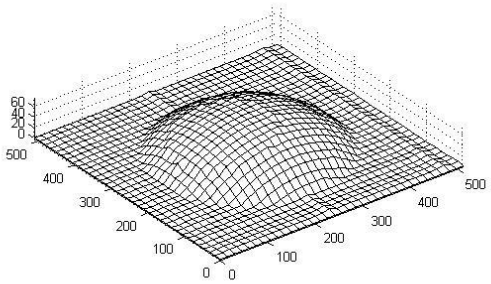

d) $\sigma = 2$

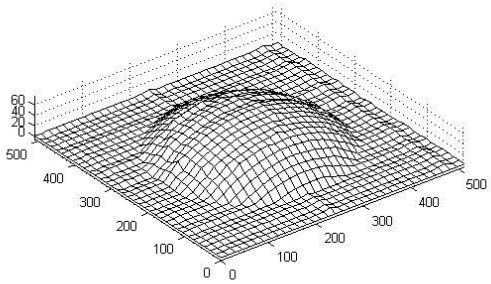

e) $\sigma = 5$

Figure 4.15: Reconstructed objects with the different standard deviations of noise.

www.manaraa.com

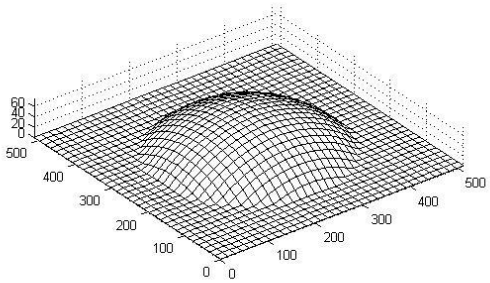

a) $\sigma = 0.1$

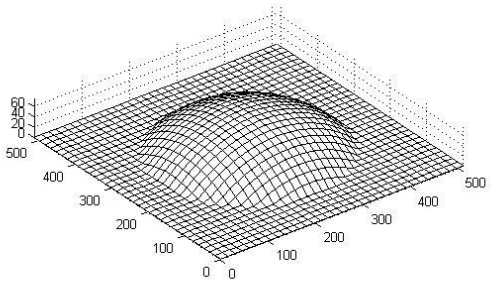

b) $\sigma = 0.5$

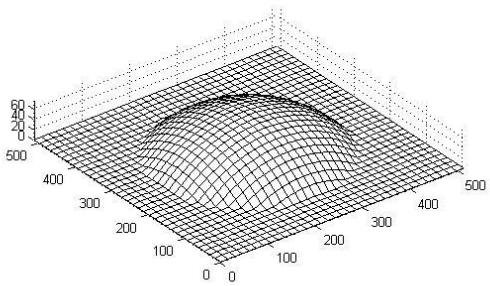

c) $\sigma = 1$

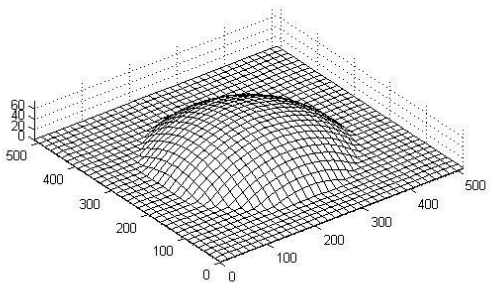

d) $\sigma = 2$

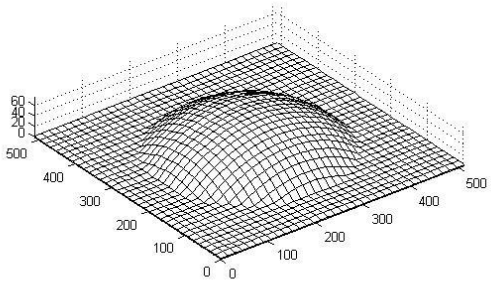

e) $\sigma = 5$

Figure 4.16: Applying mean filter on the reconstructed objects with the different standard deviations of noise.

www.manaraa.com

As we noticed in Figures 4.12 to 4.16; the method was able to reconstruct original object to an acceptable degrees. Especially after applying mean filter on the reconstructed objects.

4.2.2 Simulation of Car Roof with an Added Noise

For the car roof object, the same height as the ideal case, the same fringe period, the same maximum and minimum intensities, and the same angle of projection are used. A random noise with five distributions was added too, all of them with 0 mean but with different standard deviation values (0.1, 0.5, 1, 2, and 5). See Figures 4.17 to 4.21.

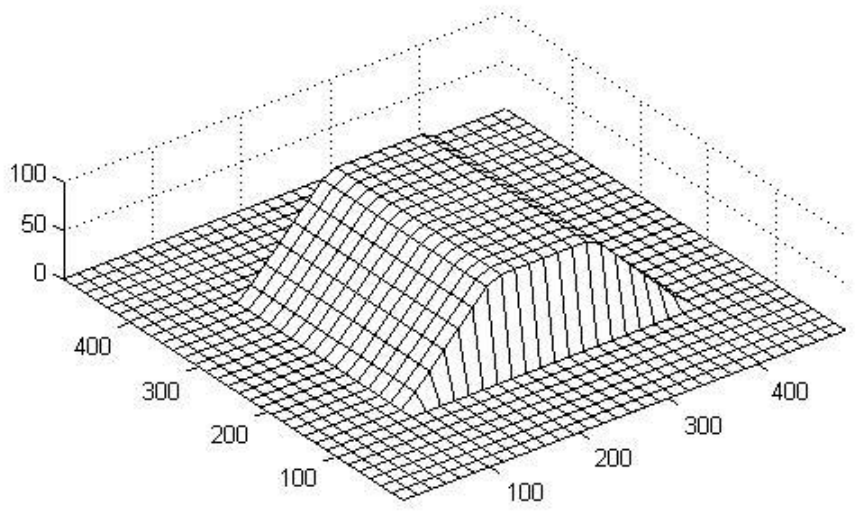

Figure 4.17: The original car roof object.

www.manaraa.com

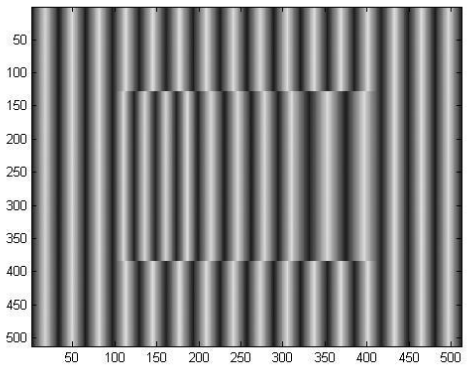

a) $\sigma = 0.1$

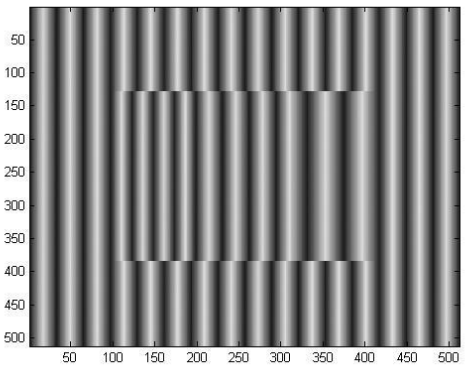

b) $\sigma = 0.5$

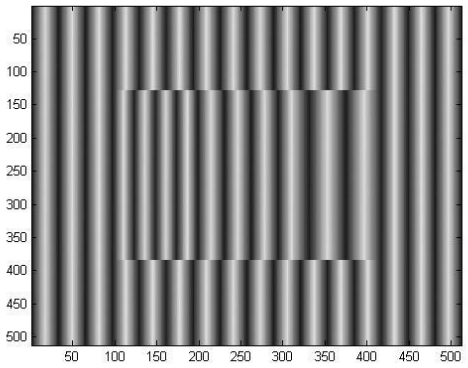

c) $\sigma = 1$

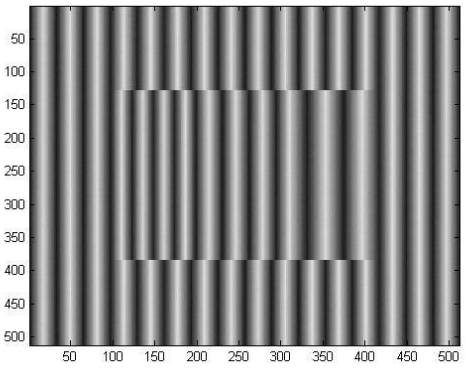

d) $\sigma = 2$

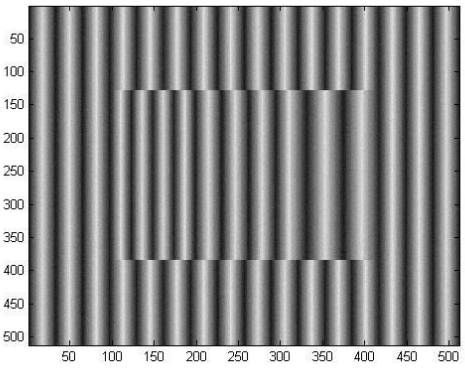

e) $\sigma = 5$

Figure 4.18: Noisy fringe patterns with different standard deviations of noise.

www.manaraa.com

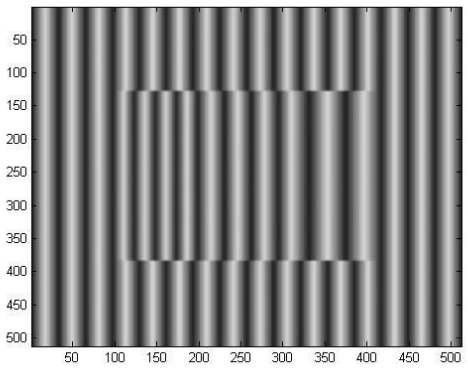

a) $\sigma = 0.1$

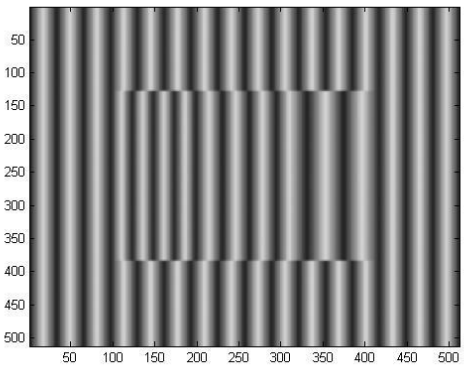

b) $\sigma = 0.5$

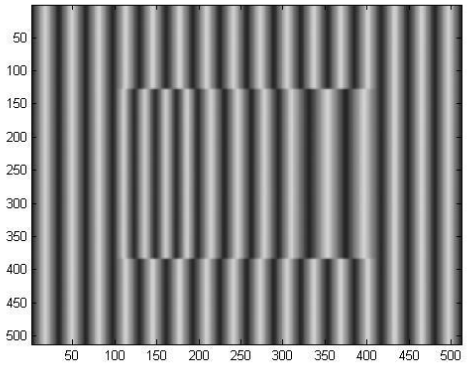

c) $\sigma = 1$

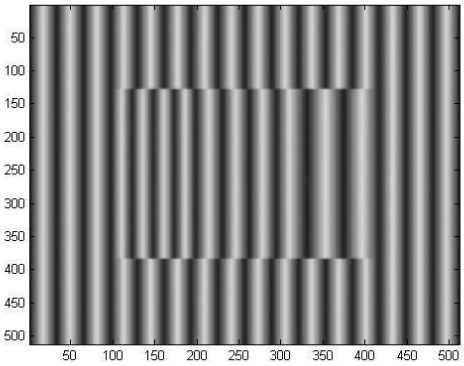

d) $\sigma = 2$

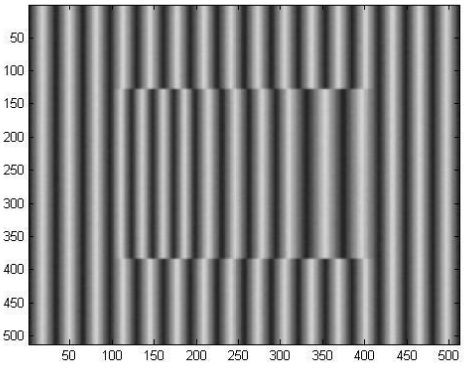

e) $\sigma = 5$

Figure 4.19: Filtered fringe patterns by weighted mean filter with the different standard deviations of noise.

www.manaraa.com

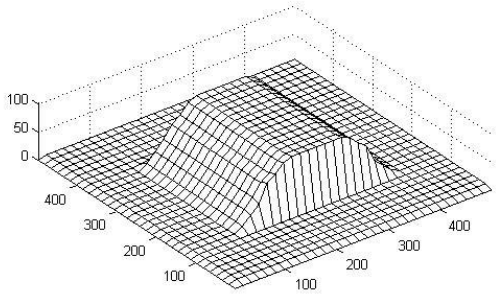

a) $\sigma = 0.1$

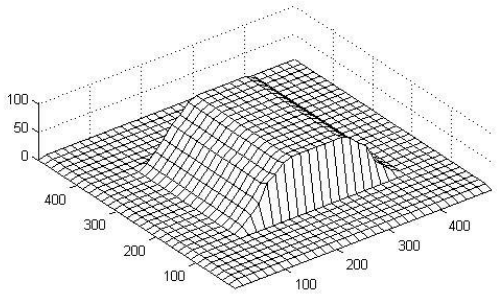

b) $\sigma = 0.5$

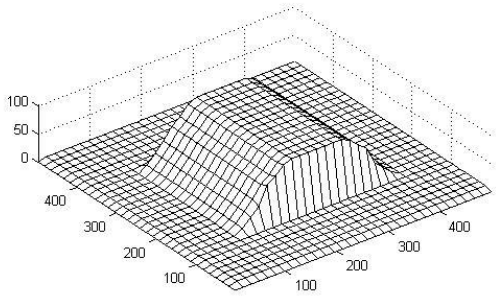

c) $\sigma = 1$

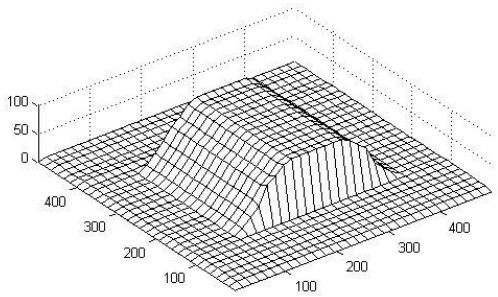

d) $\sigma = 2$

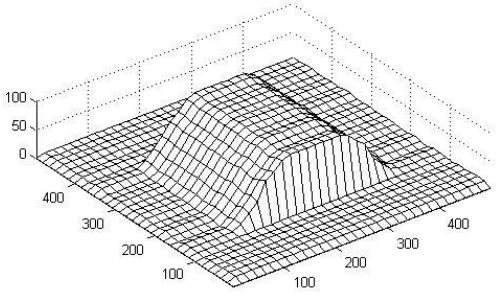

e) $\sigma = 5$

Figure 4.20: Reconstructed objects with the different standard deviations of noise.

www.manaraa.com

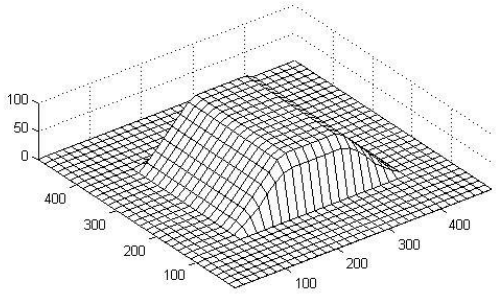

a) $\sigma = 0.1$

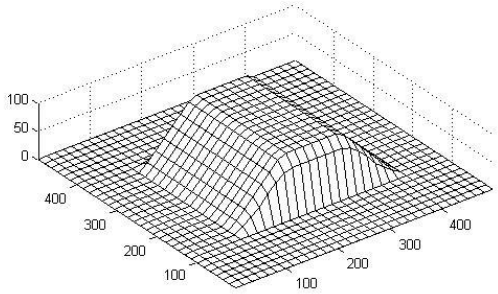

b) $\sigma = 0.5$

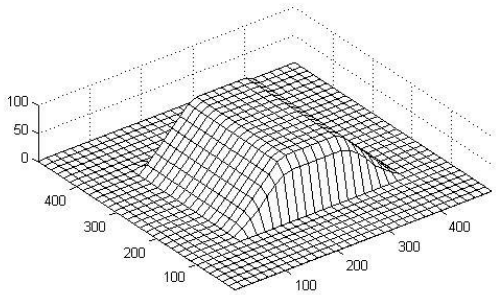

c) $\sigma = 1$

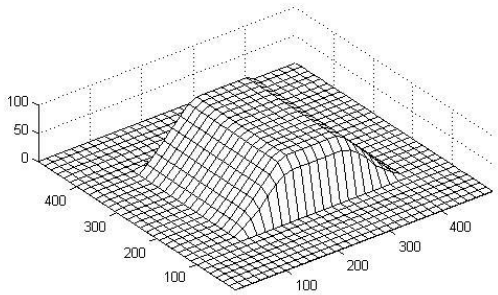

d) $\sigma = 2$

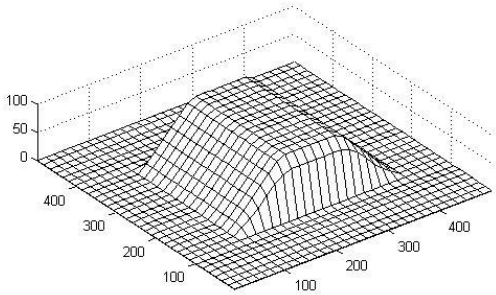

e) $\sigma = 5$

Figure 4.21: Applying mean filter on the reconstructed objects with different standard deviations of noise.

www.manaraa.com

4.2.3 Simulation of Pyramid with an Added Noise

In the same manner as previous, and for the pyramid object, the same height as the ideal case, the same fringe period, the same maximum and minimum intensities, and the same angle of projection are used. A random noise with five distributions was added too, all of them with 0 mean but with different standard deviation values (0.1, 0.5, 1, 2, and 5). See Figures 4.22 to 4.26.

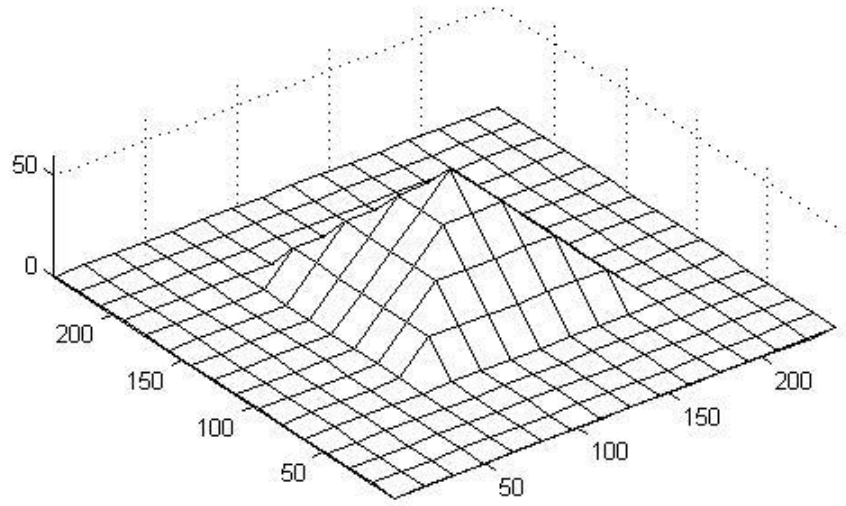

Figure 4.22: The original pyramid object.

www.manaraa.com

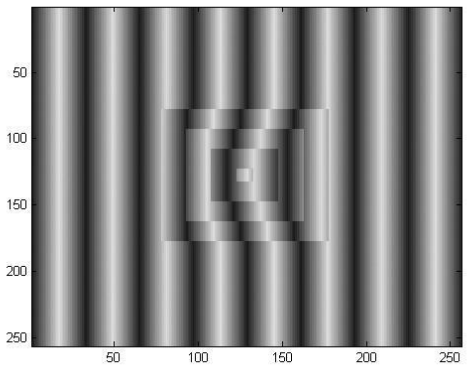

a) $\sigma = 0.1$

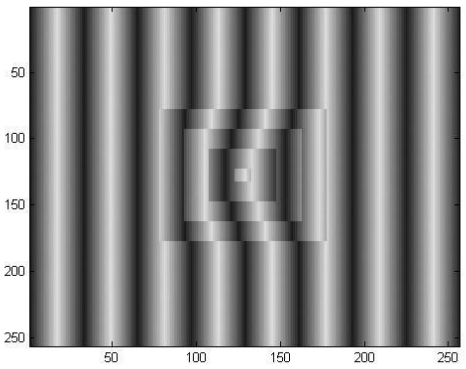

b) $\sigma = 0.5$

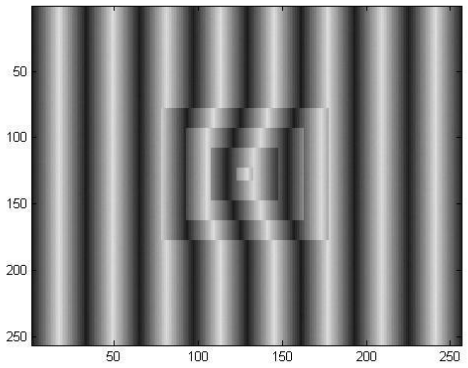

c) $\sigma = 1$

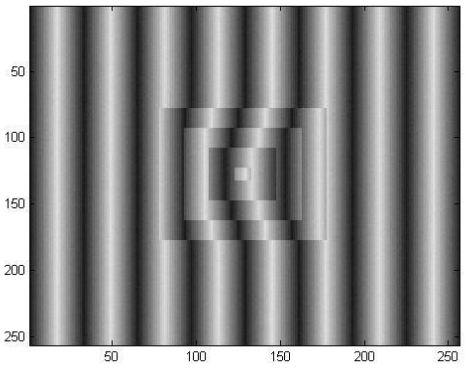

d) $\sigma = 2$

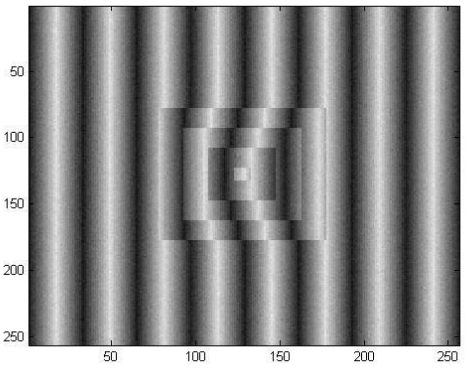

e) $\sigma = 5$

Figure 4.23: Noisy fringe patterns with different standard deviations of noise.

www.manaraa.com

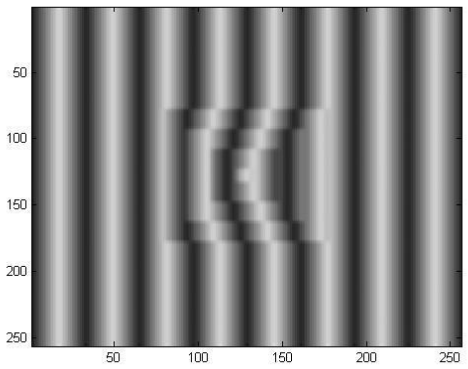

a) $\sigma = 0.1$

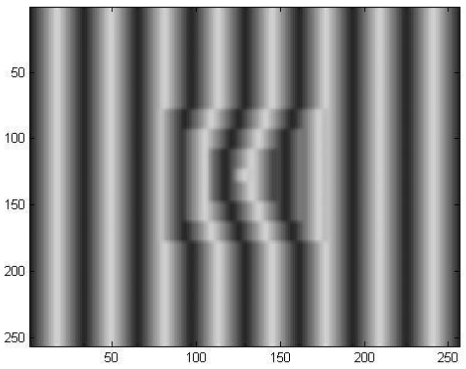

b) $\sigma = 0.5$

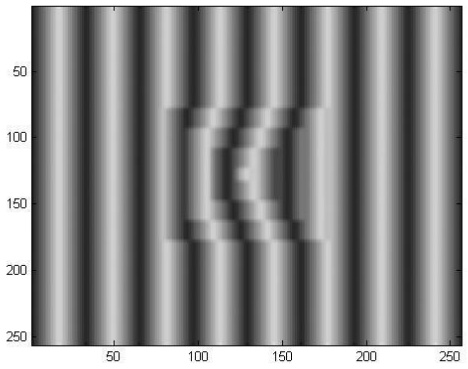

c) $\sigma = 1$

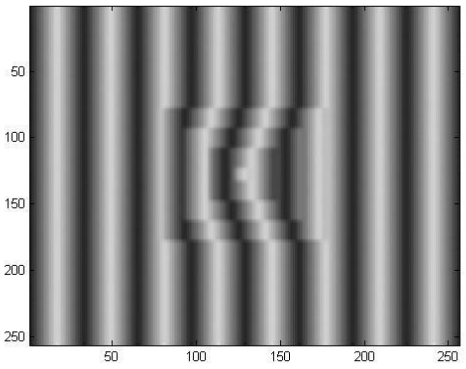

d) $\sigma = 2$

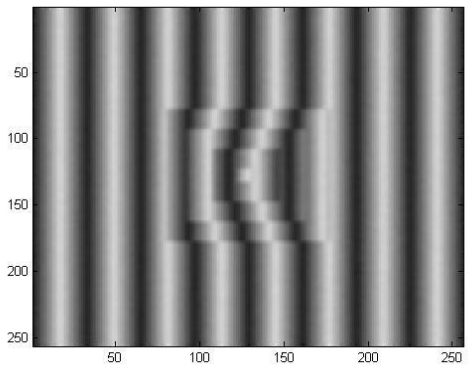

e) $\sigma = 5$

Figure 4.24: Filtered fringe patterns by weighted mean filter with the different standard deviations of noise.

www.manaraa.com

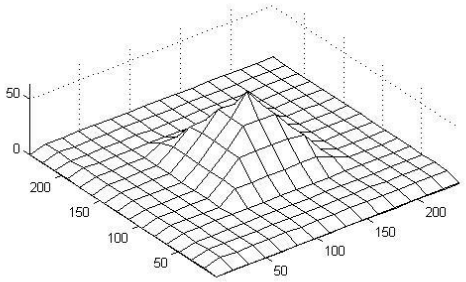

a) $\sigma = 0.1$

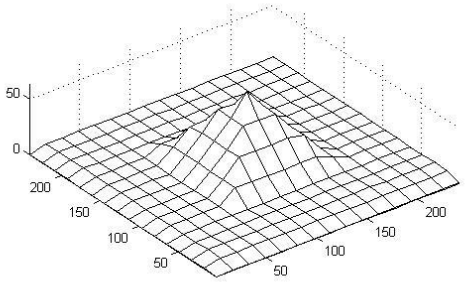

b) $\sigma = 0.5$

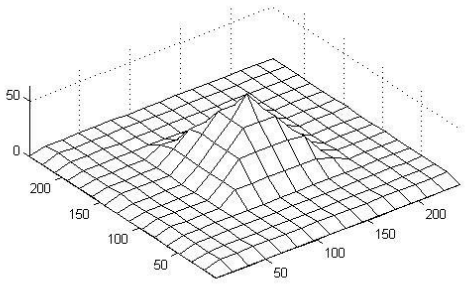

c) $\sigma = 1$

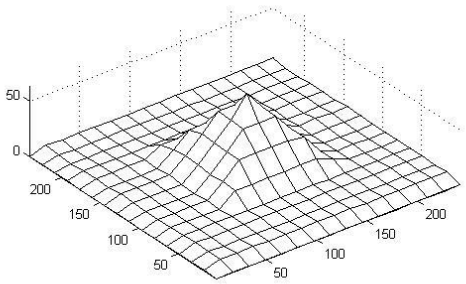

d) $\sigma = 2$

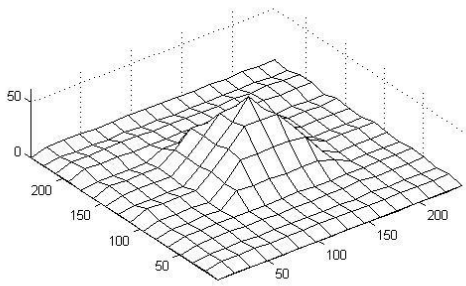

e) $\sigma = 5$

Figure 4.25: Reconstructed objects with the different standard deviations of noise.

www.manaraa.com

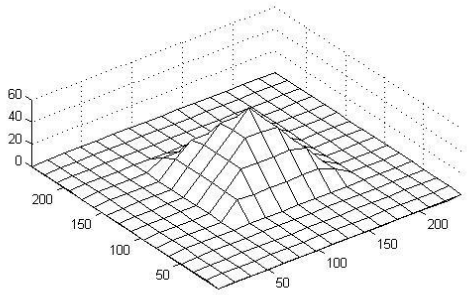

a) $\sigma = 0.1$

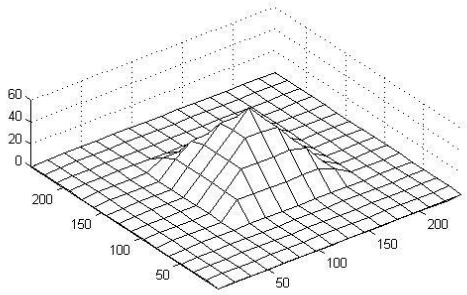

b) $\sigma = 0.5$

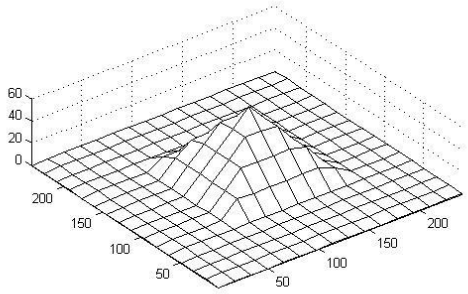

c) $\sigma = 1$

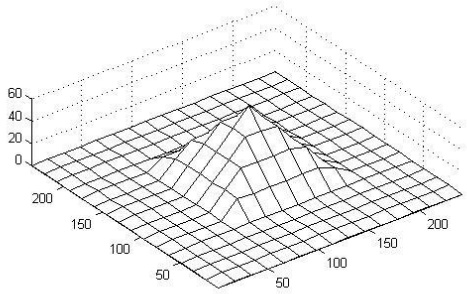

d) $\sigma = 2$

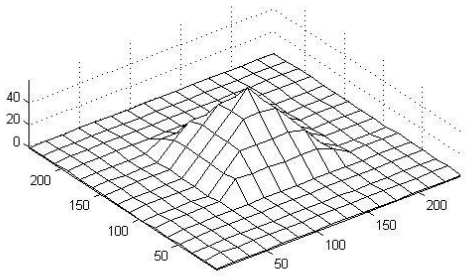

e) $\sigma = 5$

Figure 4.26: Applying mean filter on the reconstructed objects with the different standard deviations of noise.

www.manaraa.com

4.3 Error Analysis

To test the average error in the proposed technique; root mean square error (RMSE) is used which can be calculated by relation (19). Since the random noise will differ from an execution to another due to the difference in the added noise from an execution to another because it is a random process; 5 execution trials were applied for each used standard deviation and the average RMSE for the five trials was calculated.

4.3.1 Error Analysis for Semi-Sphere Simulation

To calculate the average of RMSE values for each case of random noise distributions; five trials were executed for each case. Table 4.1 shows RMSE results for each trial with all cases, and the average of RMSE values for each case.

Table 4.1: RMSE results for different trials of execution for the semi sphere object with ideal and noisy cases, and the average RMSE results for each case.

Trial	Ideal case	$\sigma = 0.1$	$\sigma = 0.5$	$\sigma = 1$	$\sigma = 2$	$\sigma = 5$
1	0.1547	0.4404	0.4058	0.4423	0.4073	0.6800
2	0.1547	0.4174	0.3998	0.4063	0.4000	0.6643
3	0.1547	0.4701	0.4051	0.4017	0.4756	0.7743
4	0.1547	0.4185	0.4406	0.4170	0.4232	0.4514
5	0.1547	0.4166	0.4217	0.4206	0.4293	0.6233
Average RMSE (Pixel)	0.1547	0.4326	0.4146	0.4176	0.4271	0.6387
RMSE:MAX Height	0.2%	0.6%	0.6%	0.6%	0.6%	0.9%

www.manaraa.com

4.3.2 Error Analysis for Car Roof Simulation

In the same manner as previous, Table 4.2 shows the RMSE results of the 5 trials of execution for each case; in addition to the average of RMSE values for each case.

Table 4.2: RMSE results for different trials of execution for the car roof object with ideal and noisy cases, and the average RMSE results for each case.

Trial	**Ideal case**	$\boldsymbol{\sigma = 0.1}$	$\boldsymbol{\sigma = 0.5}$	$\boldsymbol{\sigma = 1}$	$\boldsymbol{\sigma = 2}$	$\boldsymbol{\sigma = 5}$
1	0.0182	0.4234	0.4215	0.4531	0.4622	1.0581
2	0.0182	0.4331	0.4354	0.4261	0.4325	0.9018
3	0.0182	0.4493	0.4543	0.4347	0.4376	0.8569
4	0.0182	0.4310	0.4557	0.4412	0.5125	0.5010
5	0.0182	0.4521	0.4226	0.5556	0.6081	0.5583
Average RMSE (Pixel)	0.0182	0.4378	0.4379	0.4621	0.4906	0.7752
RMSE:MAX Height	0.02%	0.4%	0.4%	0.5%	0.5%	0.8%

4.3.3 Error Analysis for Pyramid Simulation

Table 4.3 shows the RMSE results of the 5 trials of execution for each case, in addition to the average of RMSE values for each case.

www.manaraa.com

Table 4.3: RMSE results for different trials of execution for the pyramid object with ideal and noisy cases, and the average RMSE results for each case.

Trial	Ideal case	$\sigma = 0.1$	$\sigma = 0.5$	$\sigma = 1$	$\sigma = 2$	$\sigma = 5$
1	0	0.1376	0.1433	0.1374	0.1996	0.6120
2	0	0.1384	0.1461	0.1420	0.1035	0.2790
3	0	0.1015	0.1400	0.1083	0.3109	0.4424
4	0	0.1394	0.1422	0.1915	0.2195	0.3576
5	0	0.1429	0.1414	0.1401	0.1105	0.9893
Average RMSE (Pixel)	0	0.1320	0.1426	0.1439	0.1888	0.5361
RMSE:MAX Height	0%	0.2%	0.2%	0.2%	0.3%	0.9%

Hence the method successfully measured heights of object in theoretical. In real life and practical part there are many factors that affect the results such as noise, non-linearity of both camera and projector, and non-uniform reflection of intensities. These factors were dealt in the practical experiment of this study. The practical experiment technique, factors affect the correctness of practical result, and methods of dealing with these factors are going to be discussed in the next chapter.

www.manaraa.com

Chapter 5

Practical Experiment of Triangular Fringe Projection Technique

This chapter presents the needed steps for practical 3D measurements using the proposed technique. This includes: triangular fringe patterns generation and projection, capturing the reflected image, image enhancement, and lastly heights calculations and reconstruction of object surface.

5.1 System Analysis and Experiment Procedure

A new technique has been examined and tested in the current study. The proposed system consists of a PC and a projector to project the fringe patterns, it also has a camera which is placed in a perpendicular position of the object to capture the reflected image as shown in Figure 5.1. There is an angle between the camera and the projector which is called the angle of projection. Triangular fringe patterns are projected on the object surface by the projector to test the technique of this study.

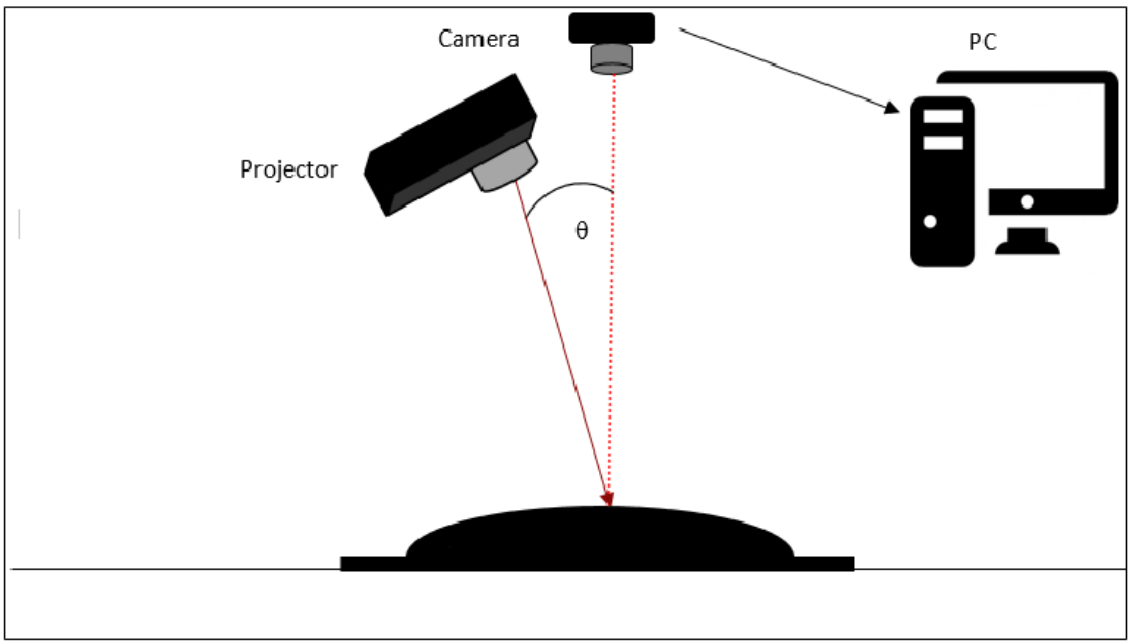

Figure 5.1: The system proposed for triangular fringe projection technique.

www.manaraa.com

It should be clarified that the mathematical derivation for the presented technique assumed a collimated light is projected from the projector. However, this is really not true, the light rays coming from the projector are not parallel, but conical, see Figure 5.2.

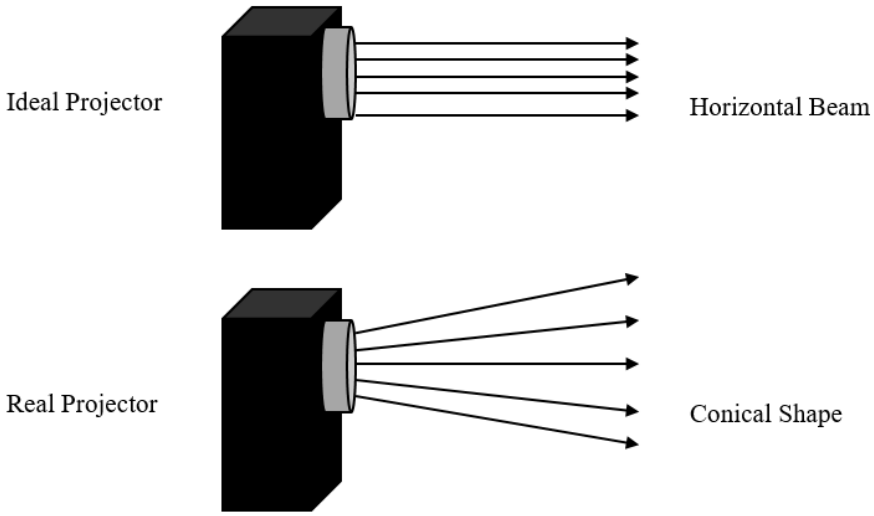

Figure 5.2: Ideal projector VS real projector rays.

Because of this problem, the mathematical derivation would not work correctly, but we can reduce the effect of this problem by projecting the beam first at a flat plane then at the object under test. By applying the algorithm to both cases and then subtracting the height distribution of the flat plane from that of the object we get the real height distribution for the object.

The first step in this technique is generating triangular fringe patterns to project them on the targeted plane by a projector. Then, the reflected image should be captured and loaded to a PC for processing. Image enhancement and noise removal techniques should be applied to the captured image; and then, calculations of triangular fringe projection technique should be applied to calculate each pixel height. Each step that is mentioned

www.manaraa.com

above should be applied on two planes. The first plane is the targeted object surface plane, while the second plane is a flat surface used as a reference plane. The depth between these two planes is calculated to eliminate the distortion in the projector described earlier. Finally the whole object is reconstructed. The research design will pass through different steps which are shown in Figure 5.3.

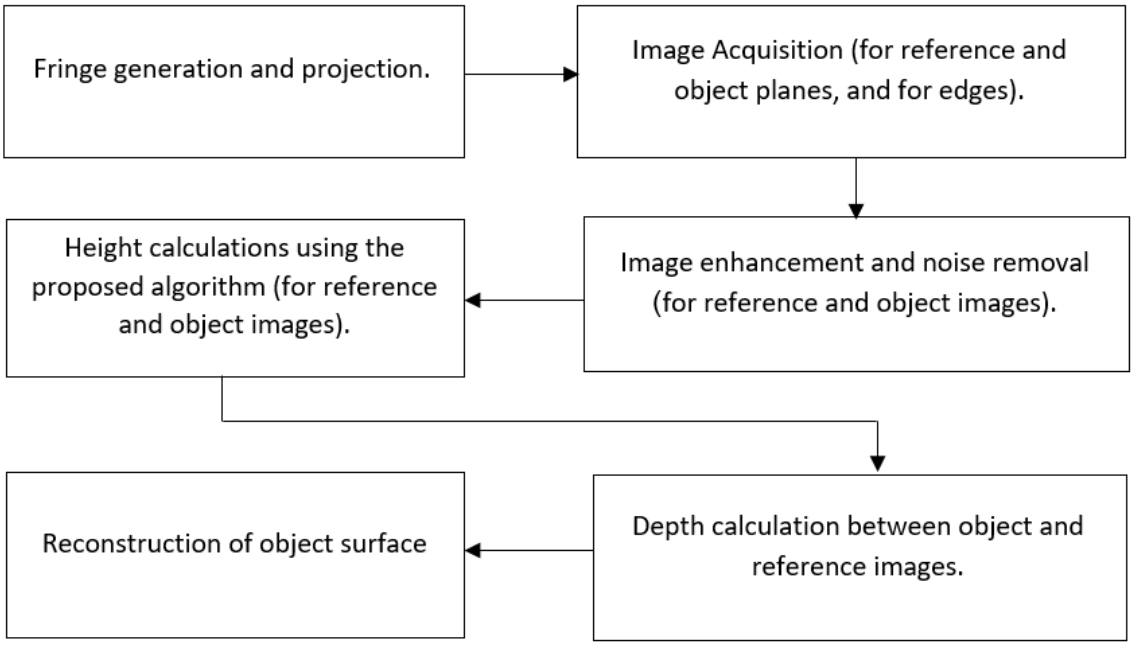

Figure 5.3: The proposed algorithm steps.

MATLAB software was used for programming purposes needed.

5.1.1 Triangular Fringe Generation and Projection, and Image Acquisition

Triangular fringe patterns in gray colour with intensity between (30) and (220) and period of 32 pixels were generated by using MATLAB software. Number of trials which were done in the current study showed that these parameters give the best performance. After fringe patterns generation, these patterns were projected onto the targeted object and onto the reference plane which should be flat. Then the reflected image of the object and reference planes modulated by fringe patterns were captured by the camera. See Figure 5.4 which is an example of triangular fringe patterns generated by MATLAB software.

www.manaraa.com

These patterns have the same parameter values (intensity between 30 and 220 and period of 32 pixel).

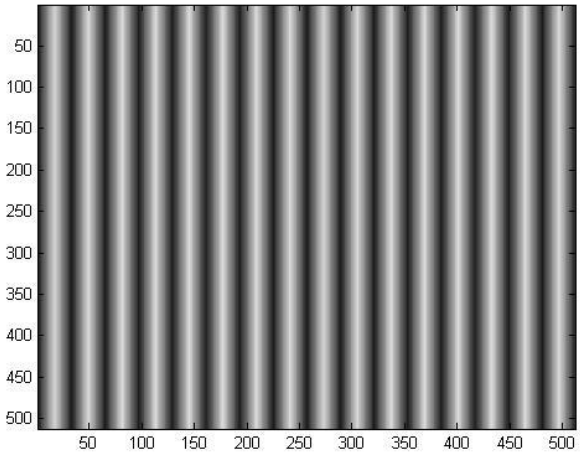

Figure 5.4: Triangular fringe patterns generated for projection.

5.1.2 Image Pre-processing

After capturing the image; the image should be prepared for the algorithm of heights calculations. The algorithm cannot be applied immediately after capturing the image because the image will suffer from noise and maybe not suitable in size …etc. There are several sources of noise such as projector light noise, camera noise, camera and projector flicker, and shadows in the picture which could happen due to the nature of the object (Li et al., 2003). The used objects in this study were painted by white to reduce the effect of noise and to reflect the most actual intensity since the white is the most suitable color for light reflection (Al-Hamdan and Hamad, 2008). The practical experiment was performed in a dark room to reduce effect of ambient light. To prepare the image it should pass throw several steps of preprocessing for image enhancement and noise removal. Firstly, the image should be cropped to suitable size and with area covering the targeted object. Secondly, the image should be converted into gray image since the camera used in this study captures images in colors (RGB), but the proposed algorithm deals with gray levels

www.manaraa.com

and does not deal with colors,. Finally, image enhancement and noise removal techniques are applied. In this research the proposed weighted mean filter was used, which computes the average value of the neighbor pixels with a specific weights for each pixel. The filter performs averaging but tries to keep edges as discussed previously in chapter 4 section 2. This depends on how far the pixel to the targeted pixel to be calculated. Moreover, setting this average value to the targeted pixel which leads to smooth the image, keep edges intensity values appropriate for the reconstruction algorithm to work correctly, and make the change of intensity between adjacent pixels more effective for calculation because it limits the distortion inherited from digital projector and digital camera. Image pre-processing steps are shown in Figure 5.5.

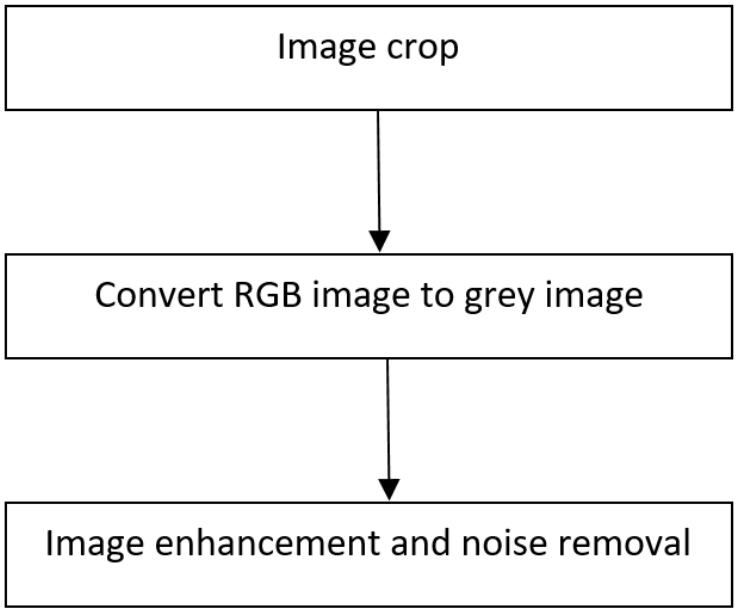

Figure 5.5: Image pre-processing steps.

It is worthy to mention here that the selected objects of this study should have a nature which does not suffer from sharp edges. Sharp edges in the object induces shadow after projection of fringe patterns. So, the fringe patterns will not reach each point in the object; thus, some points will not reflect the required intensity of fringe patterns on these points which will make all calculations wrong on these points and to all points after them in the

www.manaraa.com

same line (Lu et al., 2015). Figure 5.6 illustrates the problem of shadow in the objects that having sharp edges.

Our algorithm currently works only with smoothly changing profiles. Also, it is recommended to deal with shadow areas (in case that happened) by image processing techniques, and predict the supposed values of intensity, in case that the projection patterns reach shadow points for all points in the shadow area.

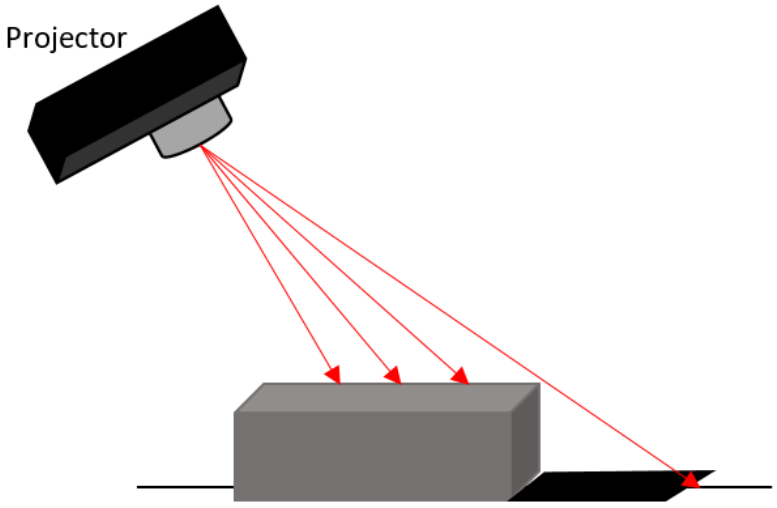

Figure 5.6: Cube object form a shadow due to its nature (the black area indicates shadow area).

5.1.3 Height Calculations

After enhancing image and removing noise; the image is ready for the proposed algorithm on it. Equation (10) and equation (18) were used, which are found and proved in chapter three to calculate the height of each pixel in the captured image starting from left to right depending on the changing of intensity for each pixel and its previous pixel until reaching the final pixel in the line. Then, repeating these calculations in similar way to all lines. After this, the heights of all pixels are calculated in the image and the object is reconstructed.

www.manaraa.com

5.1.4 Depth Calculation

The heights of reference surface (which should be a 0 height) and for object surface should be calculated. After calculating all pixels heights of the object and reference surfaces, the depth between the two surfaces should be taken to eliminate distortion in the projector as follow:

$$Height = Height_{of\ object\ surface} - Height_{\ of\ reference\ surface} \quad (21)$$

Height represents the reconstructed object which needs to be calibrated.

5.1.5 Calibration Process

After the depth calculation process, the object is reconstructed but the dimensions will not be the same of the real object due to the projector and camera properties. In addition the calculations based on pixels not on centimeters. Hence the calibration process is used to calculate the real dimensions of the object.

X-axis represents the length of the object, while Y-axis represents the width of the object, and Z-axis represents the height of the object.

X-axis can be calibrated to match the real length of the object by equation (22).

$$X_{access_calibration} = \frac{length_of_object}{size_of_X_axis} \quad (22)$$

Y-axis can be calibrated by equation (23).

www.manaraa.com

$$Y_{access_calibration} = \frac{width_of_object}{size_of_Y_axis} \quad (23)$$

Moreover, Z-axis is calculated in the same way. However, the maximum height in the reconstructed object differs from line to another. So, the average maximum height is calculated to use it for Z-axis calibration. See equation (24) and equation (25).

$$average_of_H = \frac{\sum \max(heights)}{size_of_Y_axis} \quad (24)$$

$$Z_{access_calibration} = \frac{height_of_object}{average_of_H} \quad (25)$$

One object is needed to calibrate the other object. These calibration parameters are calculated from the first object in this study (triangular shaped object) and applied to the second object (curved shaped object) to calibrate it. So from the first object we can calculate the parameters of calibration which are used to convert the second object dimensions from pixels to centimeters in all directions (length, width, and heights).

www.manaraa.com

5.1.6 Algorithm steps

Figure 5.7 summarizes all needed steps in the proposed algorithm.

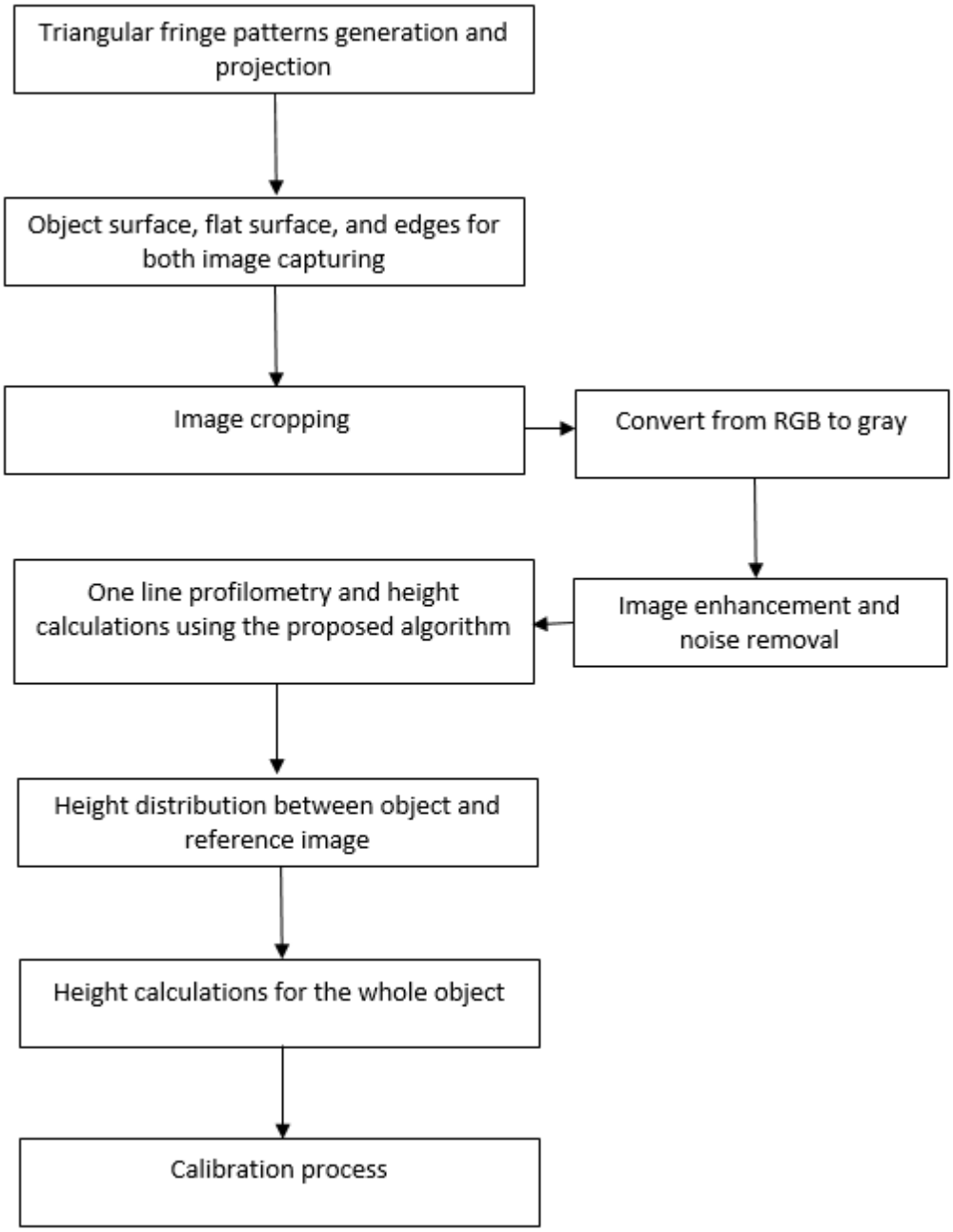

Figure 5.7: proposed algorithm needed steps.

5.2 System Setup

In this study, a setup consists of three wooden pieces (two boards and a small table). A projector, a camera, and a personal computer were used as shown in Figures 5.8 and 5.9.

www.manaraa.com

The first wooden board was used as a base for the targeted object for projecting fringe patterns on it. It was painted white to enhance the reflection of intensities. The second board was used as a floor base for the projector, camera, and computer. Furthermore, it was used to set the angle of projection between the projector and the camera by the lines which were drawn on the board to indicate the angle between the projector and the camera. The camera was placed perpendicularly with the targeted object and the projector was placed with an angle of 10 and 15 degrees with the camera (experiment trials for 10 degrees and other trials for 15 degrees); the experiments indicated that an angle of 15 degrees give better results. The small table was used to elevate up the plane of camera, and projector. The personal computer was used to generate fringe patterns. The projector was used to project the generated fringe patterns to the targeted object. The camera was used for acquisition process by capturing the reflected images after projection. Figure 5.8 shows the drawn lines on the base board for angles between camera and projector. Figure 5.9 shows the used setup in the proposed technique.

Figure 5.8: The drawn lines on the base board for angles between camera and projector.

www.manaraa.com

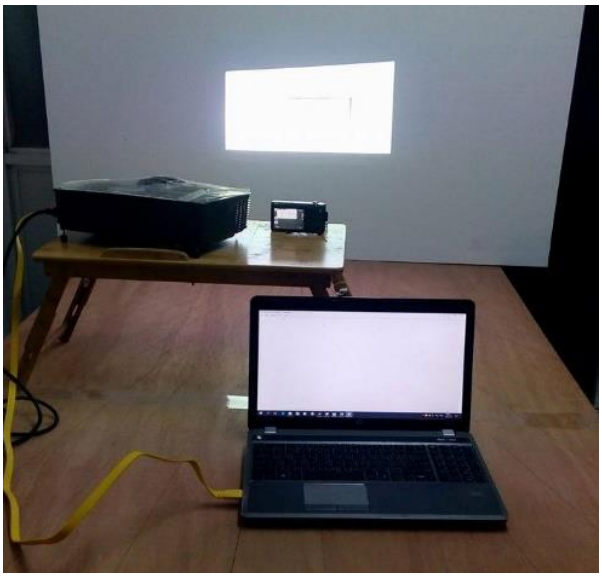

Figure 5.9: The used setup in the proposed technique.

5.3 Equipment specifications

The used projector is Optoma HD141X. The specifications of this projector are shown in table 5.1.

Table 5.1: The specifications of Optoma HD141X projector.

Optoma HD141X	
Display technology	DLP
Native Resolution	1080p 1920 x 1080
Brightness	3,000 ANSI lumens
Contrast	20,000:1
Zoom type	1.1x Manual
Projection lens	F/2.5~2.67; f=21.9~24mm, 1.1x Manual Zoom
Projection screen size	1.06 - 7.67m (41.8" - 300") Diagonal 16:9
Displayable colors	1073.4 Million

www.manaraa.com

The used camera is Samsung wb800f. The specifications of this camera are shown in table 5.2.

Table 5.2: The specifications of Samsung wb800f camera.

Samsung wb800f	
Sensor Type	1/2.3″ (Approx. 7.76mm) BSI CMOS
Effective Pixel	Approx. 16.3 Mega pixels
Total pixels	Approx. 17 Mega pixels
Lens focal Length	Samsung LENS 21x Zoom Lens f = 4.1 ~ 86.1mm (35mm film equivalent: 23 ~ 483mm)
Optical Zoom	21x Optical Zoom
Digital Zoom	Still Image mode: 1x ~ 5x Play mode: 1x ~ 9.4x (depends on image size)* Intelli-zoom: 2x

The used computer is hp ProBook 4540s. The operating system is Windows 10. MATLAB R2014a was used for all programming purposes, such as generation of triangular fringe patterns, image processing and calculations for object reconstruction; in addition to visualization of reconstructed objects. The specifications of this computer are shown in table 5.3.

Table 5.3: The specifications of hp ProBook 4540s.

hp ProBook 4540s	
RAM	4.00 GB
Processor	Intel® core ™ i3-2370M CPU @ 2.40 GHz (4 CPUs),
System type	X86-based PC

www.manaraa.com

5.4 Example of 3D Profilometry – Triangular shaped object

In this section, the needed steps for 3D profilometry are clarified. Every needed step for the reconstruction process is clarified by applying the proposed technique on triangular shape object as an example. This object is used for calibrate the second object. See Figure 5.10, the triangular shape has height of 2.5 cm, length of 15 cm, and width of 7 cm. MATLAB software was used for programming purposes.

a) Side view b) Top view

Figure 5.10: Triangular shape with side and top view.

Four images were captured, the first one was the object image after projected triangular fringe patterns on it. The second was an image of edges for the object which is needed for determining the edges of the periods to determine the corresponding slope value of each period; slope value of each period is calculated from the reference image and then assigned to the corresponding period in the object image. Here, it should be expressed that the triangular fringe patterns periods need an additional edge on the half of each period, because the pattern is triangular and there are two slopes in each period (in theory, the slope of the first half = - the slope of the second half), see Figure 5.11. The third image is the reference image which is captured after projecting the same triangular patterns (with the same period, angle and distance) on a flat surface. The fourth image is the edges image for the flat surface which is needed for determining the period edges of the reference image to calculate slope values. White objects and white surface were used

www.manaraa.com

to enhance reflection which would give better images. For projection, the triangular fringe patterns were used with maximum intensity of 220 and minimum intensity of 30, period of 32, and an angle of projection of 15 degrees.

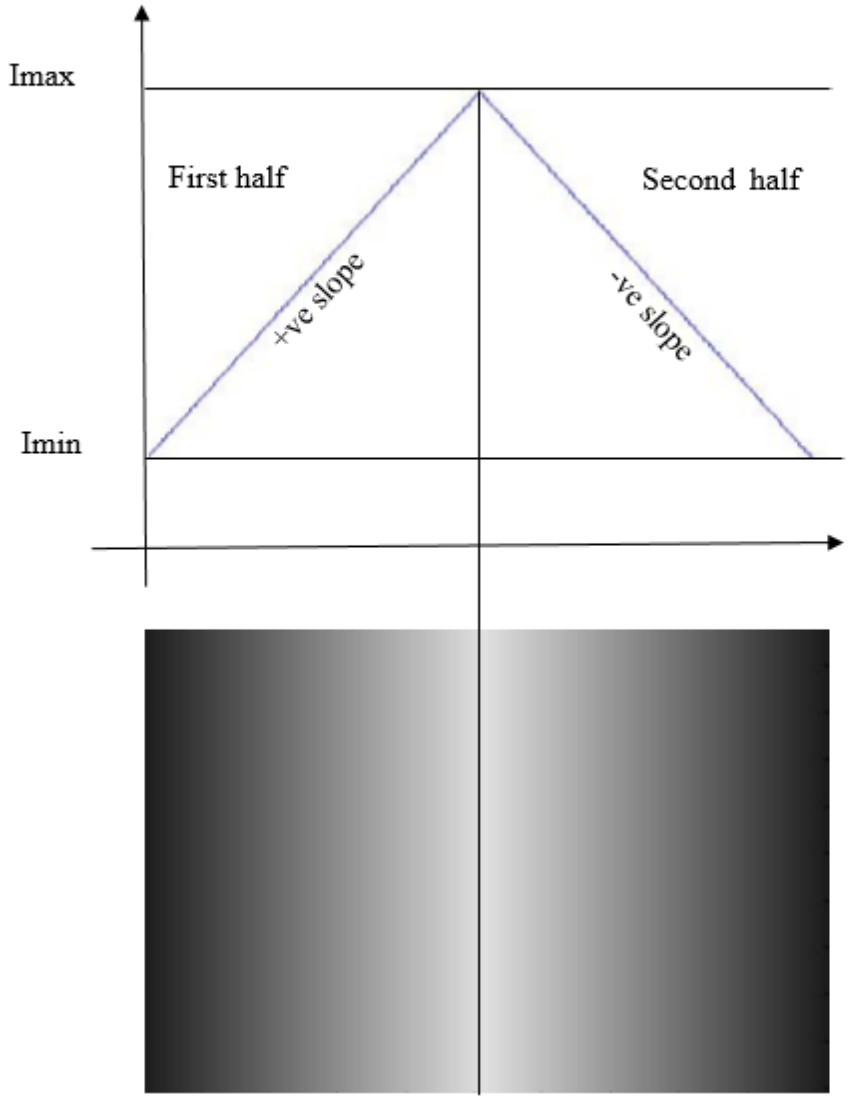

Figure 5.11: The two slopes in the same period in triangular fringe pattern.

Figure 5.12 shows the used experiment setup of this study.

www.manaraa.com

Figure 5.12: Experiment setup for image acquisition.

5.4.1 Image Reading and Cropping

In this experiment, the first step is reading the images; object image, reference image, edges of object image and edges of reference image. Then the images were cropped in an appropriate size and they should be in the same size and area to make calculations for same areas. See Figure 5.13 and Figure 5.14.

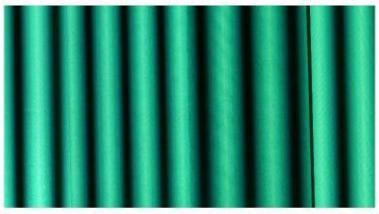

a) Object image with fringe patterns.

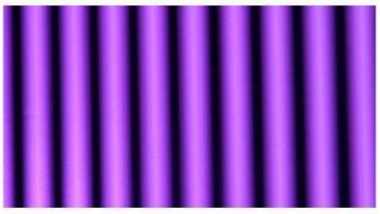

b) Reference image with fringe patterns.

Figure 5.13: Loading and cropping of fringes images.

www.manaraa.com

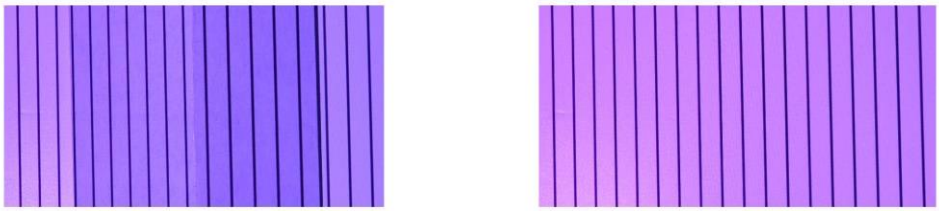

a) Object edges image. b) Reference edges image.

Figure 5.14: Loading and cropping of edges images.

5.4.2 Convert Image to Gray Level

After the images had been cropped, they were converted from RGB image to gray image because the proposed technique of this study works on gray intensities, and the camera used here records images in color format. See Figures 5.15 and 5.16.

a) Object image in gray level. b) Reference image in gray level.

Figure 5.15: Fringes image in gray level.

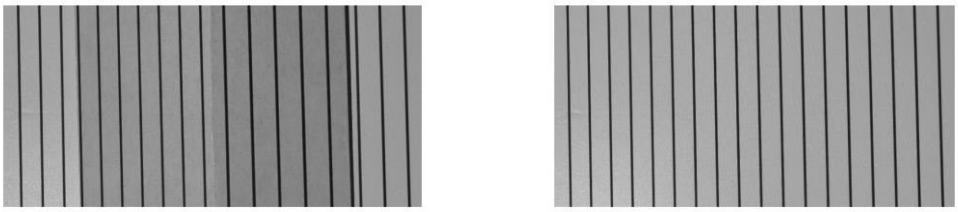

a) Object edges in gray level. b) Reference edges in gray level.

Figure 5.16: Edges images in gray level.

www.manaraa.com

5.4.3 Binarize Edges Images by Thresholding

Object edges and reference edges images are binarized by thresholding to clarify edges locations. See Figure 5.17.

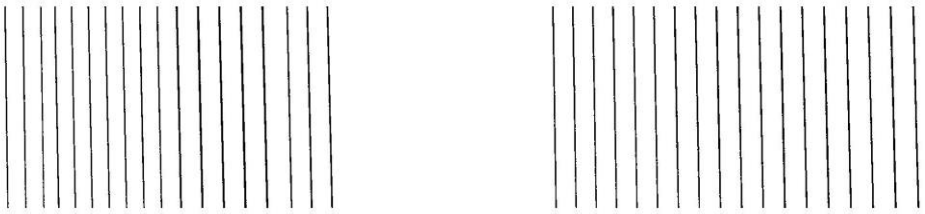

Figure 5.17: Binarize edges images by thresholding.

5.4.4 Image Enhancement and Noise Removal

The current study special 5 X 5 filter was applied on the two images (object and reference images) for removing noise and enhancing the images. See Figure 5.18.

a) Filtered object image. b) Filtered reference image.

Figure 5.18: Images after applying the filter.

5.4.5 Load One Line

Each line was worked individually, and applied the proposed algorithm of this study for line profilometry. Finally these steps were repeated to all lines. So, in this step one line was loaded from each image (should be the same line for all images) to work on it. See Figures 5.19 and 5.20.

www.manaraa.com

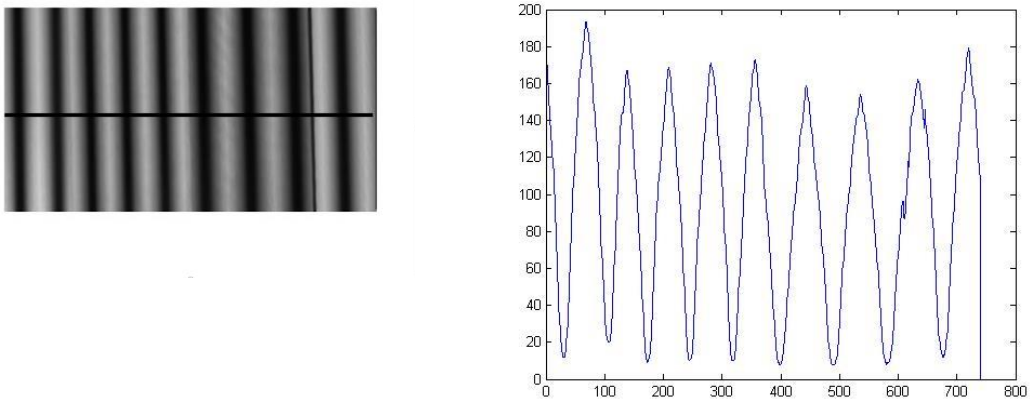

Figure 5.19: One line selection from object image at row 100 and their corresponding line intensity.

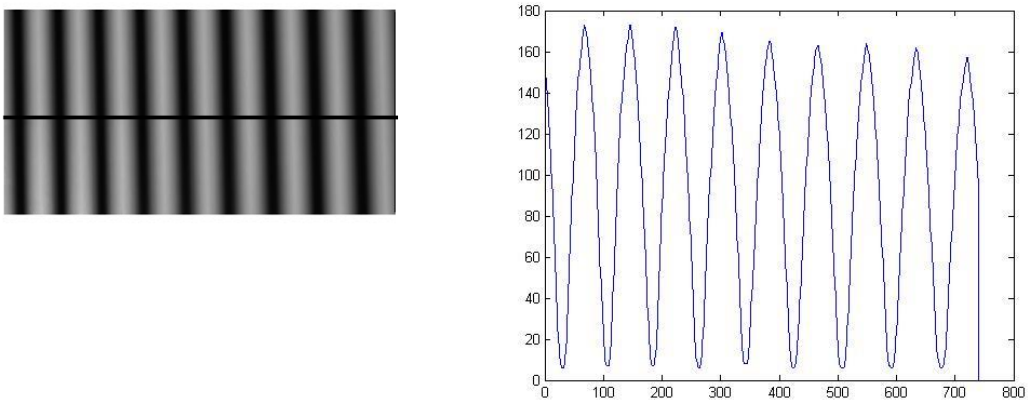

Figure 5.20: One line selection from reference image at row 100 and their corresponding line intensity.

And here as seen in Figure 5.20 triangular fringe patterns do not suffer from the abrupt change. So, no need for curve fitting as in saw-tooth algorithm which reduces computations and makes the experiment of this study more accurate.

5.4.6 Height Calculations

In this step, the heights of the pixels on the worked line were calculated depending on the proposed algorithm and equation (10) and (18) for object image and reference image. See Figure 5.21.

www.manaraa.com

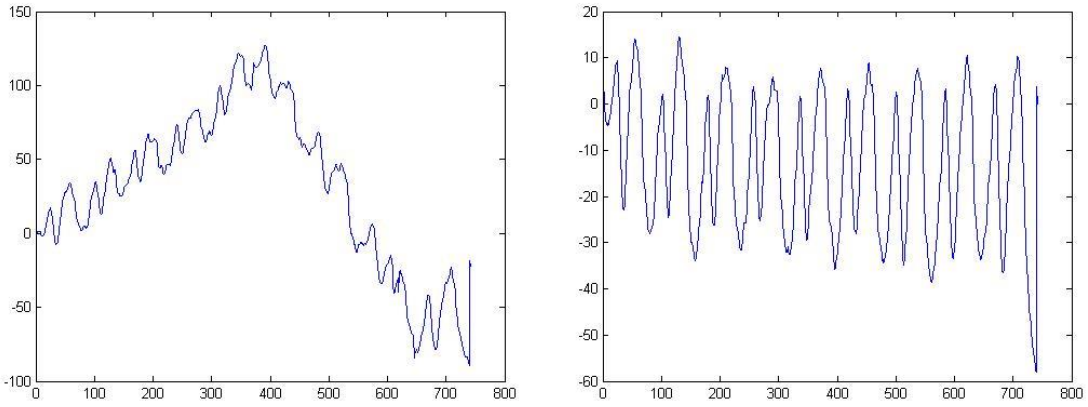

a) Reconstruction for one line of object plane.

b) Reconstruction for one line of reference plane.

Figure 5.21: Object and reference reconstruction for one line.

5.4.7 Height Distribution

After the heights for object image and reference image had been calculated individually, the depth of height was calculated to eliminate the distortion by subtracting the heights of the reference line from the heights of the object line. See Figure 5.22.

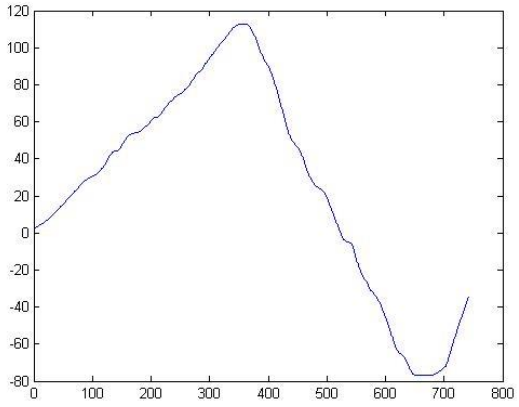

Figure 5.22: Height distribution line.

www.manaraa.com

5.4.8 Height Calculations for the Whole Object

To calculate the heights of the whole object; the applied algorithm on the line profilometry was repeated to all lines in the image and then a mean filter was applied on the reconstructed object to enhance the result. See Figure 5.23.

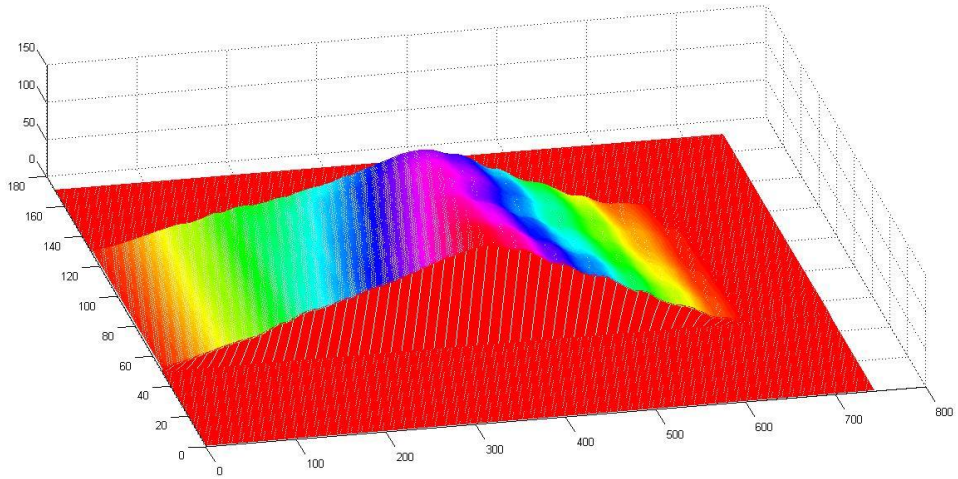

Figure 5.23: Reconstructed object.

5.4.9 Calibration process

Finally the reconstructed object was calibrated. The calibrated object is shown in Figure 5.24.

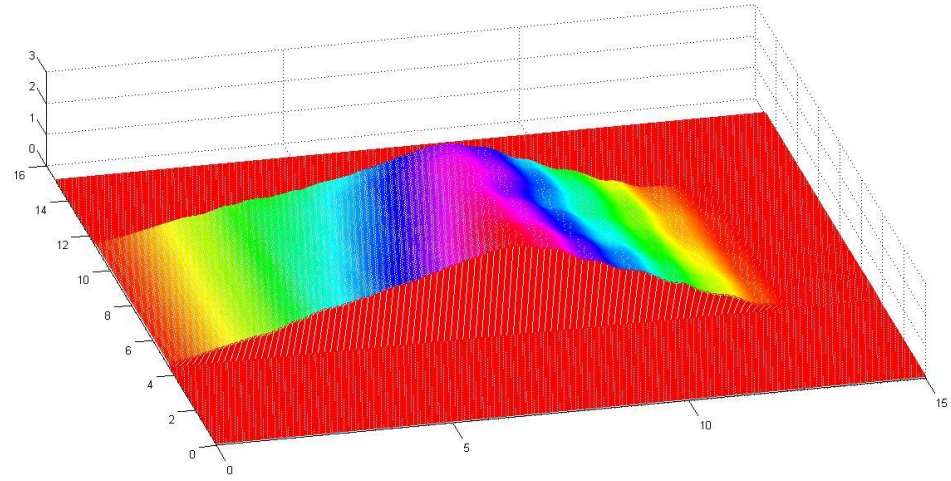

Figure 5.24: Reconstructed object after calibration.

www.manaraa.com

Hence the needed steps to reconstruct objects by using the proposed techniques were illustrated.

5.5 Practical Experiment result for curved paper object

In the previous section, an example of practical experiment of triangular fringe patterns technique was expressed with details of needed steps. The object was triangular shaped object. Triangular fringe patterns were used for projection with period of 32, maximum intensity of 220, minimum intensity of 30, and angle of projection of 15 degree between the camera and the projector. These parameters of the triangular fringe patterns showed the best results after trying many parameters to reach the best result. So, the same parameters were used for the second object (curved paper), except the period of fringe patterns which was 16 with this object, because it presented better result than 32 period. The first object (triangular shaped) was used for calibrating the second object. The second object is shown in Figure 5.25, and the visualization of the reconstruction result is shown in Figure 5.26.

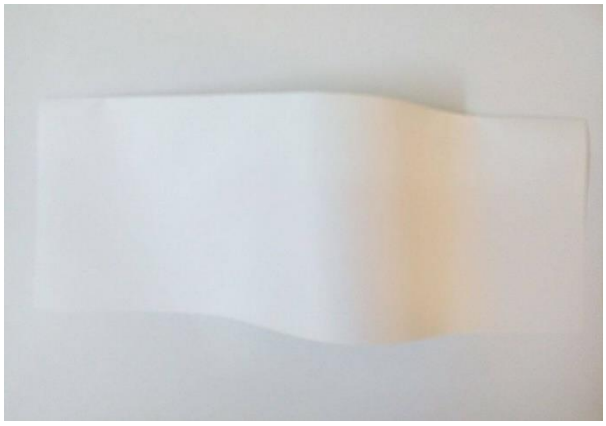

Figure 5.25: Curved paper object and its dimensions.

www.manaraa.com

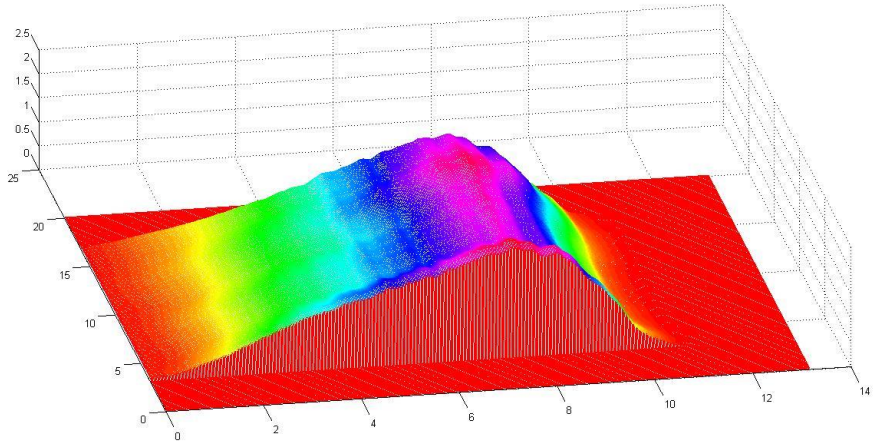

Figure 5.26: Visualization of the curved paper object after the reconstruction process.

www.manaraa.com

Chapter 6

Discussion

In this study, simulation experiments have been done and worked successfully for the proposed technique. The technique was able to reconstruct objects if the object shape has inclinations which do not suffer from the shadow problem (smoothly changing profile).

In the real life there are many factors that affect the experiment performance such as noise, room light …etc. In this study, many issues were detected which should be resolved in order to improve the performance of the proposed technique.

The first and the main issue is the relocation of camera, projector, and/or object between one capture and another; which do exist due to low resources. The proposed technique relies on capturing four images for each experiment of reconstruction as mentioned in chapter 4 (first image for the object with triangular fringe patterns, second image for the reference surface with triangular fringe patterns, third and fourth images for edges of the periods for object and reference surfaces). As mentioned in chapter five, two wooden boards and one small table were used for the setup; the first board which is painted white was used as a base for the object to project triangular fringe patterns on it. The second board was used as a base for the camera and the projector. The small table was used to elevate up the plane of the camera and the projector. None of the three pieces of setup are fixed in place. Between one capture and another, a small relocation happened every time and this affected the performance of the experiment. Best effort has been tried in this experiment to achieve fixed equipment and to prevent the relocation of them, but it is still not perfect. The solution is using a special equipment which fixes the projector, camera, and object. At the same time, these equipment can handle another problem which is the accurate setup for the angle of projection. The proposed equipment should be

www.manaraa.com

manufactured in a way that can set the angle of projection between the camera and the projector accurately. Figure 6.1 shows an example of setup that can be used as a solution for these problems.

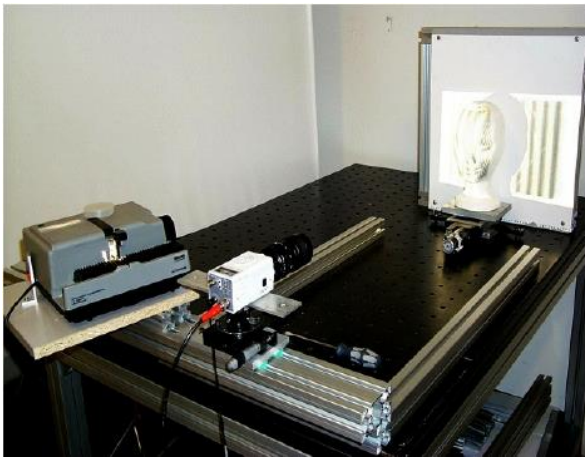

Figure 6.1: Example of a fixed setup (Sansoni and Redaelli, 2005).

Furthermore, the intensity values were different from capture to capture in the same experiment. This is due to that the projector projects a video stream of fringe projection which is not fixed picture; this causes the camera to capture different frames of this video stream; especially that the camera exposure time is more than the single channel of projection. Thus, synchronizing of the camera with the projector will reduce effect of this problem. In addition, another problem faced us is averaging of intensity values on the periods edges. Using better quality camera and projector will reduce effect of this problem and enhance the performance of the proposed technique. Better camera and projector will decrease the effect of noise and can capture high resolution images.

6.1 Comparing between Triangular and Saw-tooth Techniques in the Simulation Experiment

The proposed technique is compared with saw-tooth technique that is proposed by AL-Hamdan and Hamad (2008) in the ideal case. Table 6.1 shows the difference between RMSE results in the ideal case for car roof, and semi-sphere objects. The table indicates

www.manaraa.com

that the proposed technique gives better RMSE result with the car roof object. On contrary, it gives worse RMSE result with the semi-sphere object. These results indicate that the nature of object affects the comparison between these two techniques. Furthermore, they indicate that the proposed technique works well with reconstructing objects and it can be an alternative of saw-tooth technique.

Table 6.1: The difference between RMSE results in the ideal case for car roof, and semi-sphere objects.

	Saw-tooth	**Triangular**
	RMSE (Pixel)	**RMSE (Pixel)**
Car Roof	0.1001	0.0182
Semi sphere	0.0910	0.1547

6.2 Comparing between Triangular and Saw-tooth Techniques in the Practical Experiment

As mentioned before, in real life there are many factors affect the performance of the reconstruction process. The error of the proposed technique was calculated by the relation of RMSE. It has an RMSE equals to 0.8997cm. The saw-tooth technique which was applied by Al-Hiary (2015) has an RMSE equals to 0.5649cm which is better than the proposed technique. Applying the proposed solutions of the issues which mentioned before; will enhance the results of the proposed algorithm and will reduce errors.

On the other hand, the proposed algorithm was compared with Fourier transform and saw-tooth algorithms in terms of processing time for completing one line profilometry for each one. The needed steps for the one line profilometry are reading the images, converting

www.manaraa.com

them to gray level, image enhancement and noise removal; in addition to height calculations.

It is worthy to mention that the needed processing time differs from one machine to another, depending on the specifications of the machine (PC) that executes the program. Hence, to make a valuable comparison; the researcher should execute all algorithms on one machine to compare processing time of each algorithm. In this study, the hp ProBook 4540s PC was used in the experiment to compare algorithms. Furthermore, the processing time differs from an execution to another even with the same machine; due to the changes of CPU usage with time. So, five trials of executions have been performed for each algorithm to compute the average processing time. Table 6.2 shows the processing time needed for the five executions of each algorithm along with the average processing time.

Table 6.2: Comparing of processing time of different algorithms.

Trial	Triangular (s)	Saw-tooth (s)	Fourier Transform (s)
1	0.913	2.091	2.721
2	0.908	2.087	2.608
3	0.917	2.112	2.629
4	0.911	2.127	2.620
5	0.900	2.165	2.626
Average (s)	0.9098	2.1164	2.6408

www.manaraa.com

Figure 6.2 shows the differences in processing time for one line profilometry between the three techniques.

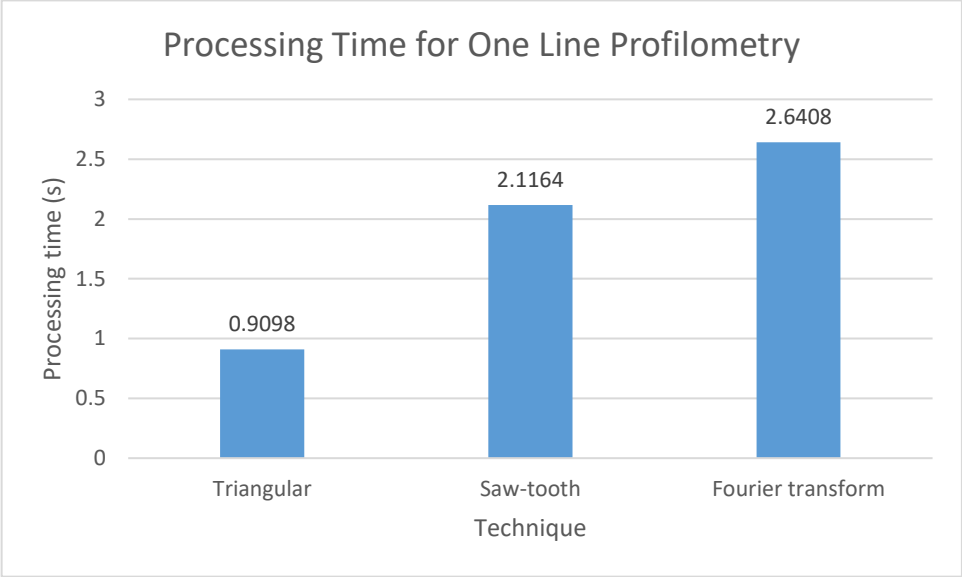

Figure 6.2: A comparison of processing time for the three techniques.

The proposed algorithm speeds up the execution time by 2.326 relative to the saw-tooth algorithm. This happens because we reduce the time needed for curve fitting in the saw-tooth algorithm, in addition to write more effective code to enhance the speed. Hence, the computations are significantly reduced in the proposed algorithm. Figure 6.3 shows a comparison in speeding up of triangular algorithm relative to saw-tooth algorithm.

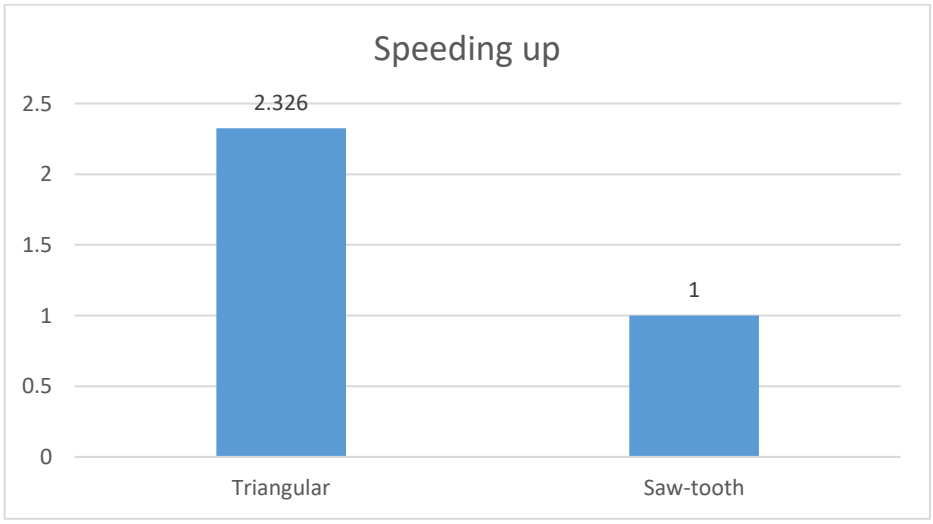

Figure 6.3: A comparison in speeding up of triangular algorithm relative to saw-tooth algorithm.

www.manaraa.com

6.3 Comparing the Used Computer with Several Computers in terms of Speed

Different computers execute the same programs with different processing time due to their specifications which differ from one computer to another. MATLAB software provides a function to compare the used computer with several computers in terms of speed. The bench function of the MATLAB software measures the execution speed of the used computer to accomplish six different tasks; and comparing the speed result with speed of several computers. Figure 6.4 shows the processing time for the used computer; in addition to the processing time of several computers for each task individually. Figure 6.5 shows the speed of the used computer; besides the speed of several computers. The longest bar is the fastest computer; in contrary, the shortest bar is the slowest computer.

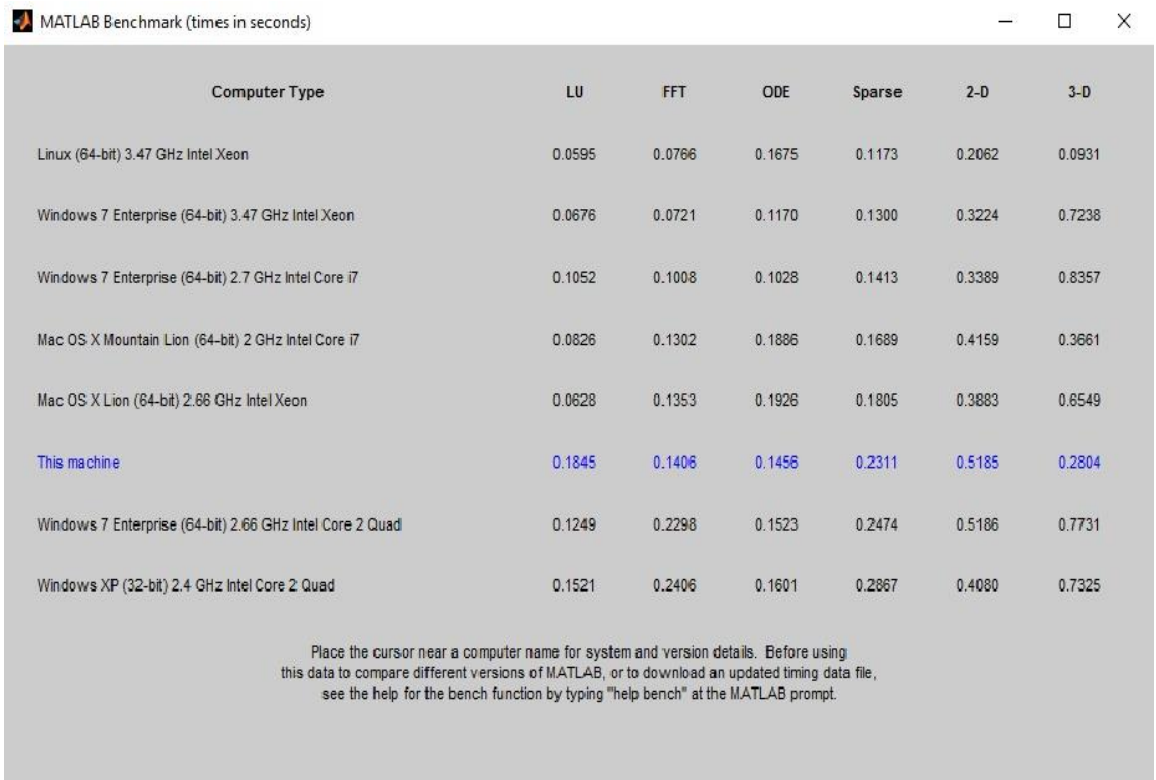

Figure 6.4: the processing time for the used computers and for several computers for each task individually.

www.manaraa.com

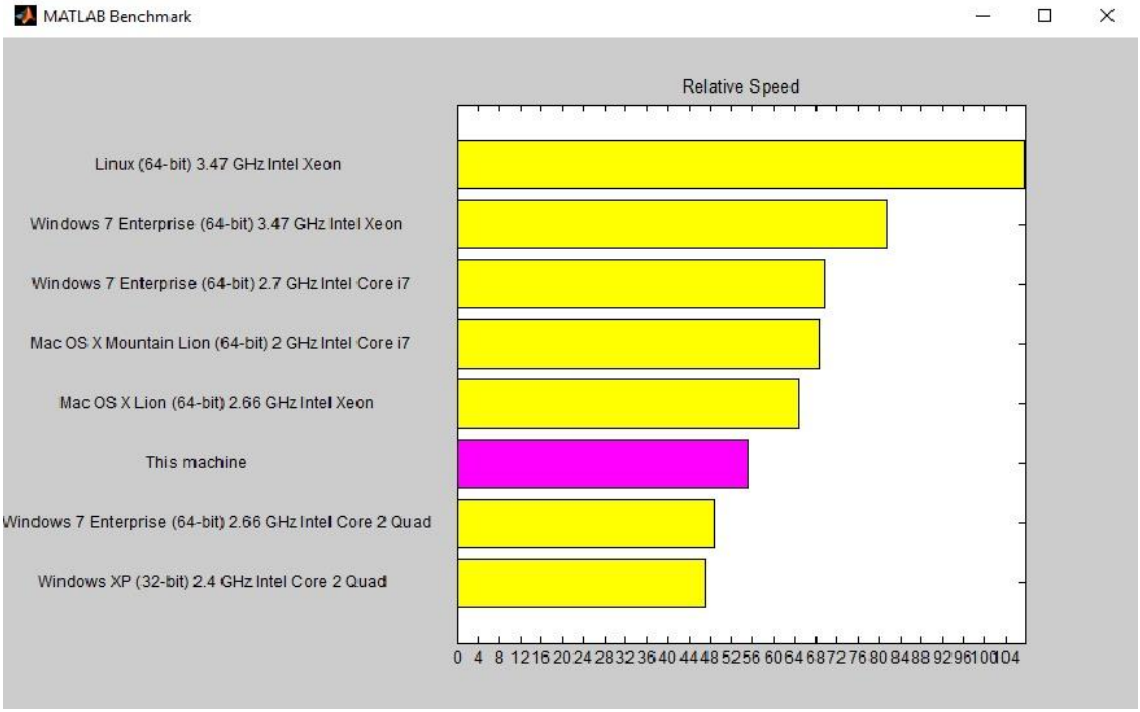

Figure 6.5: the speed of the used computer and the speed of several computers.

Hence, the use of Linux (64-bit) 3.47 GHz Intel Xeon can speed up the execution time of the proposed algorithm by 1.93. Furthermore, using a special machine which works as an embedded system for the proposed algorithm will enhance the result of speed; since the CPU will work on just one task. If this embedded system was used, there would be another proposed ideas for speeding up the execution, such as the need of capturing and reading the reference surface and the edges of this surface images; in addition to their calculations will be eliminated. Thus, they will be captured, read, and calculated only one time, and the outcomes of this image will be used for all tested objects. Thus, the execution time will be reduced; especially, the needed time of reading image function takes long time.

www.manaraa.com

Chapter 7

Conclusion, and Future Works

7.1 Conclusion

3D shape measurement techniques are widely used. In this study, triangular fringe projection technique has been studied and tested. In conclusion, a summary of findings are listed below:

- The triangular fringe patterns technique works successfully in the simulation experiment; which indicates that the computations of the technique successfully reconstruct objects.
- The root mean square error of the simulation experiment is relatively low which can be ignored.
- The triangular fringe patterns technique works fine in the practical experiment. However, it needs more work to increase the accuracy of the experiment; such as fixing the equipment of the experiment setup.
- Image enhancement and noise removal technique, such as the weighted mean filter can enhance the results of 3D profilometry.
- The triangular fringe patterns technique improves the computations of the 3D profilometry, it was proved in this study that triangular fringe patterns do not suffer from sharp drop like saw-tooth fringe patterns; which reduces the computations needed for 3D profilometry.
- The triangular fringe patterns speeds up the execution time by 2.326 relative to the saw-tooth algorithm.

www.manaraa.com

- The best performance of speed will be achieved if a special computer, with good specifications, used for only the proposed technique as an embedded system.

7.2 Future Works

- Implementing a special setup; which can fix the projector, camera, and the object in the location. Furthermore, using high quality projector and camera.
- Take into consideration the synchronization between projector, and camera when capturing images.
- Developing an embedded system for the practical experiment. Thus the computer will only work on the triangular fringe patterns technique.
- Using C language instead of MATLAB for programming purposes, because the C language takes less time in executing functions than MATLAB.

www.manaraa.com

References

Adaškevičius R. & Vasiliauskas A. 2015. 3D multicamera dental cast scanning system. *Elektronika ir Elektrotechnika,* 82**,** 49-52.

Al-Hamdan S. & Hamad H. 2008. Profile Measurement using Intensity-Based Saw-Tooth Structured Light Fringe Patterns. *ABHATH AL-YARMOUK*.

Al-Hiary S. A. A. A. 2015. *Apractical Implementation of Intensity Based Saw-Tooth Fringe Projection Technique for Surface Profilometry Measurements.* Yarmouk University.

Ayubi G. A., Ayubi J. A., Di Martino J. M. & Ferrari J. A. 2010. Pulse-width modulation in defocused three-dimensional fringe projection. *Optics letters,* 35**,** 3682-3684.

Berginc G. & Jouffroy M. Simulation of 3D laser systems. Geoscience and Remote Sensing Symposium, 2009 IEEE International, IGARSS 2009, 2009. IEEE, II-440-II-443.

Cao P. 2015. Implementation of fringe projection profilometry using triangular fringe patterns and spatial shift estimation.

Cao P., Xi J., Yu Y. & Guo Q. Digital fringe profilometry based on triangular fringe patterns and spatial shift estimation. SPIE Sensing Technology+ Applications, 2014. International Society for Optics and Photonics, 91100C-91100C-15.

Chen F., Chen X., Xie X., Feng X. & Yang L. 2013. Full-field 3D measurement using multi-camera digital image correlation system. *Optics and Lasers in Engineering,* 51**,** 1044-1052.

Chen H., Zhang J., Lv D. & Fang J. 2007. 3-D shape measurement by composite pattern projection and hybrid processing. *Optics express,* 15**,** 12318-12330.

Chen L., Quan C., Tay C. J. & Fu Y. 2005. Shape measurement using one frame projected sawtooth fringe pattern. *Optics communications,* 246**,** 275-284.

Cui Y., Schuon S., Chan D., Thrun S. & Theobalt C. 3D shape scanning with a time-of-flight camera. Computer Vision and Pattern Recognition (CVPR), 2010 IEEE Conference on, 2010. IEEE, 1173-1180.

Furukawa R. & Kawasaki H. Interactive shape acquisition using marker attached laser projector. 3-D Digital Imaging and Modeling, 2003. 3DIM 2003. Proceedings. Fourth International Conference on, 2003. IEEE, 491-498.

www.manaraa.com

Gong Y. & Zhang S. 2010. Ultrafast 3-D shape measurement with an off-the-shelf DLP projector. *Optics express,* 18**,** 19743-19754.

Gorthi S. S. & Rastogi P. 2010. Fringe projection techniques: whither we are? *Optics and lasers in engineering,* 48**,** 133-140.

Hu Y., Xi J., Chicharo J. F., Cheng W. & Yang Z. 2009. Inverse function analysis method for fringe pattern profilometry. *IEEE Transactions on Instrumentation and Measurement,* 58**,** 3305-3314.

Hu Y., Xi J., Li E., Chicharo J. & Yang Z. 2006. Three-dimensional profilometry based on shift estimation of projected fringe patterns. *Applied optics,* 45**,** 678-687.

Li J., Hassebrook L. G. & Guan C. 2003. Optimized two-frequency phase-measuring-profilometry light-sensor temporal-noise sensitivity. *JOSA A,* 20**,** 106-115.

Lu L., Xi J., Yu Y., Guo Q., Yin Y. & Song L. 2015. Shadow removal method for phase-shifting profilometry. *Applied optics,* 54**,** 6059-6064.

Muquit M. A. & Shibahara T. 2006. A high-accuracy passive 3D measurement system using phase-based image matching. *IEICE Transactions on fundamentals of electronics, communications and computer sciences,* 89**,** 686-697.

Salvi J., Fernandez S., Pribanic T. & Llado X. 2010. A state of the art in structured light patterns for surface profilometry. *Pattern recognition,* 43**,** 2666-2680.

Sansoni G. & Redaelli E. 2005. A 3D vision system based on one-shot projection and phase demodulation for fast profilometry. *Measurement Science and Technology,* 16**,** 1109.

Su X., Chen W., Zhang Q. & Chao Y. 2001. Dynamic 3-D shape measurement method based on FTP. *Optics and Lasers in Engineering,* 36**,** 49-64.

Su X. & Zhang Q. 2010. Dynamic 3-D shape measurement method: a review. *Optics and Lasers in Engineering,* 48**,** 191-204.

Takeda M. & Mutoh K. 1983. Fourier transform profilometry for the automatic measurement of 3-D object shapes. *Applied optics,* 22**,** 3977-3982.

Talebi R., Abdel-Dayem A. & Johnson J. 3-D reconstruction of objects using digital fringe projection: survey and experimental study. Proceedings of World Academy of Science, Engineering and Technology, 2013. World Academy of Science, Engineering and Technology (WASET), 720.

Telfer S. & Woodburn J. 2010. The use of 3D surface scanning for the measurement and assessment of the human foot. *Journal of foot and ankle research,* 3**,** 19.

www.manaraa.com

Wang Y. 2010. Novel Approaches in Structured Light Illumination.

Willmott C. J. & Matsuura K. 2005. Advantages of the mean absolute error (MAE) over the root mean square error (RMSE) in assessing average model performance. *Climate research,* 30**,** 79-82.

Wu K., Xi J., Yu Y. & Yang Z. 2013. 3D profile measurement based on estimation of spatial shifts between intensity ratios from multiple-step triangular patterns. *Optics and Lasers in Engineering,* 51**,** 440-445.

Xu Y., Jia S., Bao Q., Chen H. & Yang J. 2014. Recovery of absolute height from wrapped phase maps for fringe projection profilometry. *Optics express,* 22**,** 16819-16828.

Zervas M., Furlong C., Harrington E. & Dobrev I. 2011. 3D shape measurements with high-speed fringe projection and temporal phase unwrapping. *Optical Measurements, Modeling, and Metrology, Volume 5***,** 235-241.

Zhang Q.-C. & Su X.-Y. 2002. An optical measurement of vortex shape at a free surface. *Optics & Laser Technology,* 34**,** 107-113.

Zhang Z. 2012. Review of single-shot 3D shape measurement by phase calculation-based fringe projection techniques. *Optics and Lasers in Engineering,* 50**,** 1097-1106.

www.manaraa.com

قياس طبوغرافية سطح جسم عن طريق اسقاط نمط ضوئي على شكل مثلث

إعداد
محمد عبدالله محمد بواعنه

إشراف
الدكتور سامي الحمدان

ملخص

قياس الأشكال ثلاثية الأبعاد يستخدم في الكثير من التطبيقات مثل التعرف على الأجسام و التطبيقات الصناعية. أحد اشهر التقنيات المستخدمة في ذلك هي التقنيات المعتمدة على اسقاط نمط ضوئي على الجسم المراد قياس أبعاده. في هذه التقنية يتم إسقاط نمط ضوئي منظم على الجسم الهدف، و من ثم يتم التقاط الصورة المنعكسة و تحليلها بواحدة من عدة طرق لاعادة بناء الجسم الثلاثي الأبعاد. في هذه الدراسة، تم تطوير تقنية جديدة تعتمد على شدة الاضاءة لحل بعض المشاكل التي حصلت في تقنية سابقة تستخدم نمط ضوئي على شكل أسنان المنشار. هذه التقنية تعتمد على اسقاط نمط ضوئي على شكل مثلث. مجموعة من التقنيات استخدمت لتحسين الصور الملتقطة و ازالة الضوضاء عنها لتحسين النتائج. يتم تحليل الصور المحسنة لحساب ارتفاعات الجسم المراد قياس طبوغرافيته باستخدام القوانين المثلثية. في هذه الدراسة تم اجراء تجربة محاكاة و تجربة اخرى عملية لاختبار التقنية الجديدة. في تجربة المحاكاة تم اختبار التقنية على ثلاثة أجسام ذات اسطح تغيرات ارتفاعاتها سلسة على حالتين: الحالة الأولى حالة خالية من الضوضاء و الحالة الثانية مع اضافة ضوضاء. بينما تم استخدام جسمين آخرين مشابهين لأجسام المحاكاة في الخصائص في التجربة العملية. تم تصميم مرشح لتحسين الصور الملتقطة لتعطي نتيجة أفضل و هو مرشح المعدل المرجح. التقنية استطاعت اعادة بناء الأجسام الاصلية لدرجة مقبولة، و كان الجذر التربيعي لمعدل مربع الأخطاء (RMSE) في تجربة المحاكاة قليل نسبيا. ايضا تم عمل تجربة عملية يستخدم فيها جهاز عرض لاسقاط النمط الضوئي، الة تصوير لالتقاط الصورة المنعكسة عن الجسم الهدف، و حاسب الي لانشاء النمط الضوئي و تخزين الصورة المنعكسة و معالجتها و تحليلها. نتيجة اعادة البناء في الجزء العملي كانت غير مرضية نسبيا، قيمة الجذر التربيعي لمعدل مربع الأخطاء كانت 0.8997. التقنية الجديدة سرَعت وقت التنفيذ بمقدار 2.326 نسبة الى التقنية التي تستخدم نمط ضوئي على شكل أسنان المنشار في الجزء العملي. تم استخدام برمجية MATLAB لجميع الأغراض البرمجية في هذه الدراسة مثل تنفيذ تجربة المحاكاة، انشاء النمط الضوئي ...الخ.

المنارة للاستشارات
www.manaraa.com